UCRL-ID-131619

Hydro Schemes and Reactive Flow in 1D and 2D

Kurt H. P. H. Sinz and David L. Morgan, Jr.

June 30, 1998

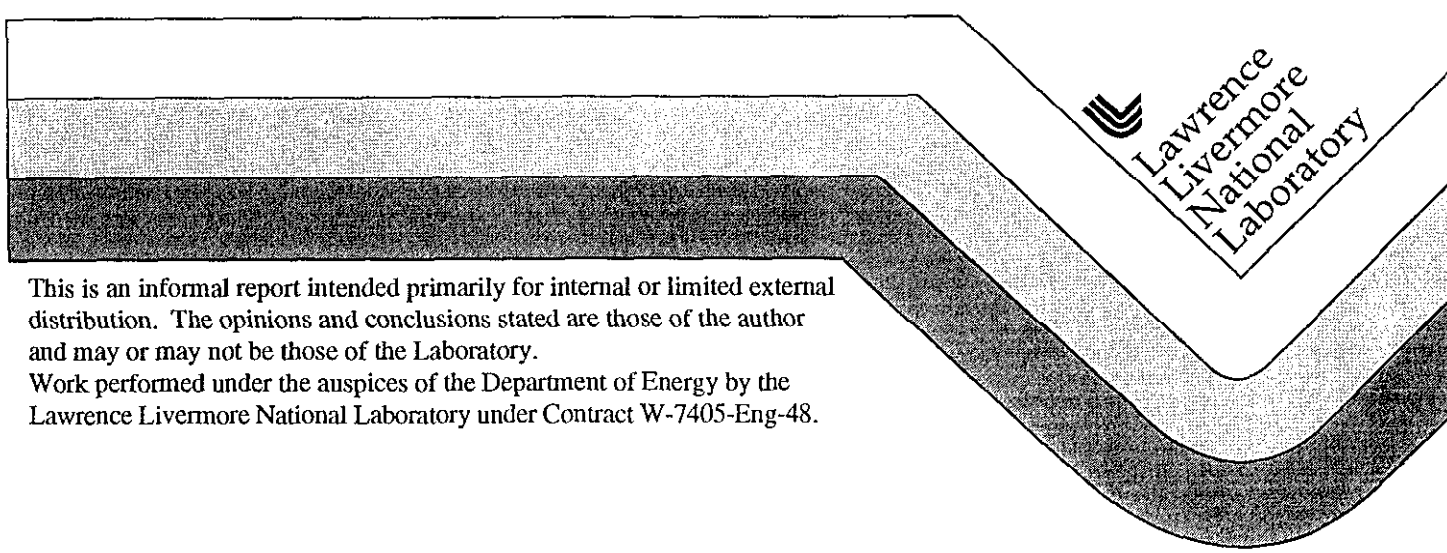

Hydro Schemes and Reactive Flow in 1D and 2D

30 June, 1998

Kurt H. P. H. Sinz and David L. Morgan, Jr.

Abstract

The behavior of the implementation of Craig Tarver's reactive flow model for high explosives in a hydro code[1] is investigated. The model produces the correct shock propagation rates. The effects of geometry, zoning and artificial viscosity are compared in one (1D) and two (2D) dimensions. Sensitivities to the solution scheme of the hydro equations are also investigated. A comparison with an experimentally verified, analytic theory is presented for the speed of spherically diverging reactive flow fronts. We show that for LX-14 the reactive flow results obey that theory and a lag of about 1.5 to 2.0 mm is produced in a spherical system in about 5 cm of travel from the origin compared to programmed burn. Reactive flow is shown to produce a more strongly developed Mach stem than does conventional, programmed lighting assisted by beta burn. The reactive flow results appear to be close to convergence for zone sizes of 1/16 mm. Several numerical anomalies in code/model behavior are shown and their limited effects are discussed. Some one-dimensional results for LX-17 are also briefly discussed.

Introduction

The use of a reactive flow model for the propagation of HE detonation is becoming more important for B Division work. We have analyzed the results of a series of hydro code runs involving reactive flow to investigate their validity and to determine the code input parameters that produce the most reliable results. The particular reactive flow model employed was that originated by Craig Tarver.[1]

The runs fall into three categories, all involving LX-14 as the explosive. In the first category, we modeled propagation in a cylinder, lit in the middle of one end, in which a plastic sphere was imbedded. This problem is discussed in Section I "Application in 2D" and was the configuration of a recent experiment in which x-radiographs of the detonation front were obtained as it proceeded around the sphere and underwent a self interaction on the far side. No comparisons to experiment are presented here; our intent was to investigate the code's treatment of reactive flow for this geometry. In the second category, discussed in Section II "Test Runs in 1D," both the lighting and the mesh properties were such that quantities varied in only one dimension. We used a slab mesh with planar lighting, a cylindrical mesh with lighting on the axis, and a spherical mesh with lighting at the origin. In the third category, discussed in Section III "Comparison of

1D and 2D Results," we looked at propagation in one half of a sphere of HE, lit at a point, calculated in cylindrical geometry. Section IV "Reactive flow and Programmed Burn," compares reactive flow with programmed burn in the 2D application problem. In addition, we did some 1D test runs with LX-17 that are summarized in Section II.

In all cases, the HE was divided into a detonator section consisting of HE modeled with programmed-burn (pbHE) and a main portion consisting of HE modeled with reactive flow (rfHE). This was done because rfHE requires something to initiate it. The pbHE extended 4 mm from the lighting plane, line, or point, and we used the same EOS, density, and detonation speed for it as for the reaction products in the rfHE (McAbee-Haselman High CJ), except that we gave it 50% more initial chemical energy. This means of lighting appeared adequate to get the rfHE detonation proceeding in a reasonable fashion within a few millimeters and was better than others we had tried. However, this may not be a realistic representation of a detonator. Finding an optimal representation of a detonator when one may not want to model its actual characteristics, may be worthy of a future effort.

When reactive flow is employed, the hydrodynamics code solves chemical reaction rate equations to determine the release rate of explosive energy as it depends on specific energy and density of the HE. (See Tarver, et al.[1]) The shock front accompanying the detonation compresses and heats the unexploded HE (which has its own EOS), thereby causing the energy release through the induced chemical reactions. In principle, at least, this is a more realistic procedure than modeling detonation by programmed lighting and/or beta burn. In particular, it offers the possibility of direct calculation of detonation velocity dependence on detonation front curvature and curvature of the detonation path. Further, it should give a more accurate representation of interacting detonation fronts.

In this study, we varied the numerical means of solving the hydrodynamics equations employed by the code, characteristics of the artificial viscosity, and the mesh spacing for each of the problem categories. We determined the effects of variations in numerical method and geometry on the detonation speed, pressure pulse wave shape, energy release, impulse, calculational noise, and Mach stem shape. All artificial viscosities employed were monotonic and used a coefficient for the quadratic term of 0.75 and a coefficient of 0.5 for the linear term.

In summary, we have determined the following. A zone size of about 1/16 mm or smaller is required for accurate results at least in the first four or five cm of detonation-front travel after ignition to establish the pulse. With this zoning, the detonation speed is calculated accurately, as well as its dependence on detonation front curvature. Once detonation has begun in reactive-flow LX-14 in a diverging geometry, it takes a few millimeters to a few centimeters of travel for the detonation to achieve a steady state in regard to peak pressure, pulse shape and detonation speed. This distance is a function of the zone size as well. For a stationary Eulerian mesh, as we employed, the most accurate

and least noisy detonation fronts (considering all orientations relative to the mesh) were produced by a numerical algorithm that face-centered the velocities (as opposed to corner-centered) along with an artificial viscosity that was both tensorial and monotonic. Such a combination also gave a reasonable Mach stem in the application problem. ALE numerics on a stationary Eulerian mesh appeared to offer no substantial improvement except for a slightly better agreement of the position of the shock front with a 1D calculation. However, near the forty-five degree line the ALE hydro shared the same pronounced noise characteristics that were seen in the corner-centered hydro.

Some anomalies were found, including a small high-pressure region (localized in two dimensions) that followed the detonation front and left a low-pressure "wake" (for face centered, scalar Q), as well as fronts with pressure spikes ("checkerboarding," see below).

I. Application in 2D

First, we discuss a series of calculations in 2D as indicated above. We took this opportunity to test the effects of velocity centering in the mesh as well as the artificial viscosity. The problem is shown in Fig. A1 and the Mach stem in Fig. A2. For all runs, zoning details are given in Tables I and II which summarize the pertinent runs that we made.

Table I. Runs Made in 2D (Cylindrically symmetric mesh, point lighting).

Run	Comment	Dz (mm)	Dr (mm)	Metric no.	Velocity centering	Artificial Viscosity
m16	*	1/16	1/16	0	Face	Scalar
m23	*%	1/16	1/16	0	Face	Tensor
m26	S	1/32	1/32	0	Face	Scalar
m41	*	1/16	1/16	2	Corner	Scalar
m42	*%	1/16	1/16	2	Corner	Tensor
m43	%	1/32	1/32	0	Face	Tensor
m47		1/32	1/32	2	Corner	Scalar
m49	%	1/32	1/32	2	Corner	Tensor
m64	>	1/32	1/32	-2	Corner	Scalar
m82	*% #	1/16	1/16	0	Face	Tensor

Table II. Runs Made in 1D (Corner-centered velocities).

Run	Comment	Dz (mm)	Dr (mm)	Metric no.	Geometry	Indep. Variable	Lighting
m38		1/16	1/16	1	planar	z	plane
m39		1/16	1/16	2	cylindrical	r	axis
m40		3deg	1/16	3	spherical	R	point
m50		1/64	1/16	1	planar	z	plane
m54	$	3deg	1/16→1/8	3	spherical	R	point
m55	$	3deg	1/32→1/8	3	spherical	R	point
m56	$	3deg	1/32→1/16	3	spherical	R	point
m58	$	3deg	1/16→1/4	3	spherical	R	point
m65		3deg	1/32	3	spherical	R	point

Comments: Tables I and II

* Model of full cylindrical x-ray experiment, rest are HE only.

\# HE is fully programmed burn (LX-14, Haselman '93, high CJ, normal parameters, shadow velocity = detonation velocity = 0.883 cm/μs), rest are reactive flow with programmed burn detonator.

% Had tensor Q, rest had scalar Q.

$ Smaller zones for 0.0–0.4cm, larger zones for 2.0–20.0 cm with ratio zoning in between to match. See also Table III.

r Cylindrical radius.

R Spherical radius.

> Eulerian mesh with "ALE" hydro-numerics.

S The "ruby solitaire" appeared in this run.

Axis lighting: lighting is along the axis of the cylinder.

The detonators are 0.4 cm of programmed burn LX-14 (Haselman '93, high CJ) with 1.5 times the normal value of the energy parameter.

Values of the energy release time chosen for programmed burn HE (detonators and main HE when applicable) are close to 1.5 × zone-size/(0.883 cm/μs). When the zone size was smaller than the reaction zone thickness, then the reaction zone thickness was used instead of the zone-size.

All problems with a dimensionality of 1 have three zones in the cross direction.

Effect of Artificial Viscosity

Runs were made on the full 2D problem to ascertain the effect of the artificial viscosity (Q). For face-centered velocities, the effect of a scalar Q (m16) was compared with a tensorial Q (run m23). The Mach stem area for run m23 (Fig. A3) shows greater smoothness than for run m16 (Fig. A2). An overlay of the contours from these two runs (Fig. A4) shows that the effect of a tensorial viscosity is limited to greater contour smoothness with no appreciable effect on the shock propagation rate. A certain amount of undercutting of the backside of the Mach stem near the axis in run m16 is also evident. This effect is removed by the tensorial Q as can also be seen by comparing Figs. A2 and A3.

The same comparison was made for corner centered velocities using runs m41 (scalar Q) and m42 (tensorial Q). Fig. A5 shows the overlay of the contours. The tensorial Q is seen to very slightly advance the shock in time compared to the scalar Q. The amount of shift is comparable to the amplitude of the noise in the contours of run m16 compared to run m23 (Fig. A4). We note here that tensorial Q aggravates checkerboarding for corner-centered velocities which is discussed next. The least overall noise, however, occurs for face-centered velocities and monotonic, tensorial Q.

Checkerboarding

In 2D calculations it was noted that patterns of alternate zones ahead of the main shock reach high pressures (Fig. A2). This "checkerboarding" seems to be highly dependent upon the choice of velocity centering. For face-centered velocities, checkerboarding is more dominant near the axis as illustrated in Fig. A2. Figure A6 illustrates checkerboarding near the forty-five degree line in a problem that uses corner-centered velocities. There the high-pressure zones appear in diagonally linked chains ahead of the main shock. These leading overshoots tend to be more severe in the corner centered zoning on the forty-five degree line than in the face-centered zoning near the axis. However, when the velocities are corner centered, the checkerboarding disappears near the axis of symmetry. Spherical expansions that were calculated on a 2D mesh showed the same checkerboarding pattern so that no effect due to boundary conditions in run m41 is indicated. For face-centered velocities with scalar Q, a single (or sometimes a few) clustered high pressure zones were seen to wander through the mesh near the shock front. We consider this to be a form of checkerboarding. The change in the checkerboarding and in the general computational noise by the artificial viscosity is discussed below.

Effect of Velocity Centering in 2D

Figure A7 shows an overlay of the contours of m23 (face centered, tensor Q) and m41 (corner centered, scalar Q). The agreement between these two runs is remarkable.

Checkerboarding in m41 is limited to the 45 degree direction and is absent near the axis — unlike m16 (face-centered velocities, scalar Q). We, therefore, conclude that the centering of the velocities does not affect the signal propagation in a major way. Face-centered velocities, however, are more prone to develop noise that produces some structure near the axis on the backside of the shock. This feature can be reduced by using a tensorial Q. Sphericity and pressure levels seem to be unaffected by the centering when identical zoning is used.

II. Test Runs in 1D

While performing the 2D runs, several questions arose about the timing of the shock. To answer these questions a number of calculations were performed in 1D because of zoning flexibility and the ability to run physically large problem with ease. We first explore the reactive flow as a function of geometry.

Shock Velocity and Pulse Shape as a Function of Geometry

Problems m38–m40 permitted comparison for planar, as well as cylindrically and spherically divergent shocks. Typical shock pressures were 0.38 Mb. Shock positions were defined by finding the position of pressure values of 0.05 Mb in the shock front. A test was made to determine whether defining the shock position at the point where the shock pressure reaches half maximum would affect our results. No appreciable difference was found.

Figure B1 shows snap shots of the pressure profiles for the three geometries at corresponding times. It is apparent that spherical divergence gives a more severe rarefaction behind the shock which results in a more sharply peaked pressure pulse than in the planar case. We also note the general broadening of all pulses in time as well as the constant pressure level between the back of the pulse and the closed boundary. The initiation region occupies only 0.4 cm of the 20 cm system length or radius. Figures B2, B3 and B4 show qualitatively similar behavior in the density, energy and particle velocity respectively.

In the cylindrical case, a simple exponential fits the release portion of the pulse. Fits for the other release profiles were not attempted but they do not appear to be substantially different in character. This fact, together with the simple appearance of the solutions, is strongly suggestive of the existence of at least an approximate analytic solution for this problem.

A close-up of the final pulses in Fig. B5 shows several features of interest. A flattening at the top of the planar pulse is clearly visible. The planar shock also shows noise. We

hypothesize that this noise is related to the "checkerboarding" that we have seen in 2D. It is also clear that the pulses are displaced with respect to one another. Fig B6 shows the shock positions as a function of time for the three geometries. Differentiation of these positions with respect to time leads to Figs. B7 and B8. The latter figure is the result of a single pass with a simple, area-preserving, smoothing algorithm. The last figure makes it clear that asymptotically the shock speeds approach the same value irrespective of the geometry. The differences, however, appear to lie in the time required to reach this speed from the initial lighting. Fig. B9 shows the difference in shock positions between the planar case and the other two cases. It is apparent that the differences in position approach an asymptotic value. Again, we see that differences in velocity and hence position are limited to the early shock formation in divergent geometries.

To attempt to gain an understanding of why this should be the case when in all three geometries the HE is lit with programmed burn for a material thickness of 0.4 cm (about 0.45 μs) we look at several factors that appear to be related to this issue. Fig. B10 shows a succession of pressure profiles both in slab geometry (solid lines) and in spherically divergent geometry (dashed lines). We see in the spherically divergent case that the pressure in the pulse takes some time to build up after entering the reactive flow region; this, despite the fact that pressures in the programmed burn portion are initially higher. For the slab geometry case, there is only a relatively small change in the pulse shape and amplitude resulting from the transition from programmed burn to reactive flow.

We attribute this behavior to the greater steepness of the release behind the shock in divergent geometries which decays the pulse from behind in the early stages of shock formation. This phenomenon delays the formation of the full shock, thus lowering the early shock pressures. These lower pressures, in turn, cause the pulse to travel more slowly, thus leading to the time delay in establishing the full shock speed.

Zone Refinement

Several problems were calculated that run to 20 cm in about 22 μs. These runs were made in 1D in spherically diverging geometry to facilitate tests of zoning sensitivity especially in the regions of early ignition and pulse formation. These runs are m40, m54, m55, m56, m58 and m65 (see Table III). The programmed lighting occurs in the first 4mm in uniform zoning as described earlier. Outside a radius of 2 cm the radial zoning is again uniform with the two regions being linked by zoning of constant ratio. The results are compared in Fig. C1. The more finely zoned calculations (m40, m56 and m65) show some amount of overshoot at the leading edge of the pulse. Overshoots for run m65 (320 zones/cm) at early times reach pressure levels of 0.518 Mb well in excess of 0.381 Mb for this high explosive. No explanation has been found so far for this behavior which

seems to have a slight effect on the propagation. The overshoots for the other calculations do not seem to have a noticeable effect on the propagation rate.

Fig. C2 shows how much the shock front in these calculations lags behind the shock position predicted by programmed burn using the ideal detonation speed. The lag clearly approaches an asymptotic value (ordinate in Fig. C2) in the range of one to two mm for zoning of 160 zones/cm or finer while zoning of 80 zones/cm and less produces noticeably more noise and a greater lag behind the programmed burn.

Theory and Experiment in Spherical Divergence

Green and James[2] conducted experiments to test a theory by Wood and Kirkwood[3] that relates the propagation rate of burn fronts in high explosives to the curvature of the wave front. In particular, they find that the propagation rate is given by $dR/dt = D_\infty(1-3.5a^*/R)$ where R is the radius of curvature of the burn front in spherical geometry and a^* is the thickness of the reaction zone. D_∞ is the asymptotic propagation rate of the detonation front and t is the time.

A convenient method for fitting this equation to our numerical results was constructed as follows. First, the relation was integrated to obtain $R = R_0 + D_\infty t - 3.5D_\infty a^* \int dt/R$ where all integration constants have been absorbed into R_0. The integral in this relation was evaluated using the numerical time integral of the calculated shock positions (such as shown in Fig. B6). A least squares fit of this integral relation to the numerical shock positions versus time was obtained which yielded values for a^* and D_∞. Compared to finding the full analytic integral of the differential equation, this representation has the advantage that these constants of interest appear only linearly. The limits of the domain of the fits in all cases were taken to be 0.8 μs and 22.5 μs. The reason for the choice of the lower limit is that at this time the detonation pulse has pretty well emerged from the domain that is governed by the programmed burn portion of the high explosive and has fully entered the regime of reactive flow. The resulting values are given in Table III. We note that the inferred reaction zone thickness a^* is a model parameter and not an input of experimental data. We further note, however, that the values in the table for a^* are within the range of values for the reaction zone thickness for HMX explosives given in Ref. 4. Furthermore, all inferred values of the asymptotic detonation speed agree well with the nominal value of 0.883 cm/μs for the equation-of-state, density and chemical energy that we used.

Fits of the analytic shock speeds to the derivatives of the shock positions versus time are given in Figs. C3, C4, and C5 for problems m40, m56, and m65. The slightly higher asymptotic shock speed for m65 (see table) is probably related to the linearity in the

shock position that is seen in Fig. C2 beginning at a time of about 8 μs. This time correlates with the observation of substantial overshoots in the pressure profiles discussed above and visible in Fig. C1 (black curve).

Table III. Coefficients for the analytic fit to the shock speeds for LX-14 in spherical divergence. D_∞ is the asymptotic shock speed, a* is the inferred thickness of the reaction zone. The number of zones per centimeter is given for radii less than 0.4 cm and greater than 2 cm. The two zoning regions are joined by ratio zoning. The number of zones per inferred reaction zone thickness is also given as is the radius of the reaction front from the origin when the shock speed D reaches 99% of its asymptotic value D_∞.

Problem	D_∞ (cm/μs)	a* (mm)	#zones/cm R < 0.4cm	#zones/cm R > 2cm	#zones/ a*	R(cm) at D/D_∞=0.99
m65	0.8844	0.1163	320	320	3.7	4.07
m40	0.8826	0.1271	160	160	2.0	4.45
m56	0.8831	0.1307	320	160	2.1	4.58
m55	0.8809	0.1341	320	80	1.1	4.69
m54	0.8801	0.1390	160	80	1.1	4.87
m58	0.8826	0.1822	160	40	0.7	6.38

Several similar runs were conducted for LX-17 (TATB). Time constraints and some code problems, probably related to boundary conditions in the metric version of the code when small spherical sectors are used, prevented us from achieving definitive results. This is a rarely used code option and a code fix was not pursued. However, our preliminary results indicate that LX-17 behaves in a very similar way with 99% of the detonation velocity being achieved in about 26 μs after the initial lighting.

III. Comparison of 1D and 2D Results

Several comparisons were made of a 1D problem run on 2D meshes as well as a 1D spherical mesh. The problem is the same as already discussed above in the section of 1D problems. To establish a basis for comparison, Fig. D1 shows a close-up of the pressure front for several 1D spherical problems as a function of the zoning at a time of about 2.134 μs. Apparently problem m65 with its zoning of 1/32 mm has achieved a high degree of convergence.

A number of problems were calculated as illustrated in Fig. D2 which shows an overlay of pressure contours for runs m26 and m47 calculated on a stationary Eulerian mesh. As noted in the figure caption, this plot compares face-centered velocities with corner-centered velocities, both for a scalar Q. The corner-centered run displays checkerboarding which does not appear to affect sphericity. For purposes of comparing

results with true 1D runs, plotlines were chosen in this type of 2D problem at about the 3 and 87 degree lines and at the 45 degree line. The next figures show comparisons between several such profile plots.

Figures D3 and D4 show the effect of scalar and tensorial Q for face-centered and corner-centered velocities respectively. The noise in the latter plot is on the forty-five degree line and it is amplified by using a tensorial Q as already mentioned. The face-centered case also shows some amount of phase difference resulting from the choice of Q at this early time of 2.13 μs.

Figure D5 compares pressure profiles resulting from using ALE hydro and standard hydro, both with corner-centered velocities and Eulerian meshes. Both suffer from severe noise on the forty-five degree line to a comparable degree. The ALE hydro enjoys as its only advantage the fact that the near-axis and the forty-five degree results are more nearly coincident.

Figure D6 shows the comparison between ALE hydro and the 1D run m65 which was performed on a spherical, metric mesh. Except for overshoots, sphericity and the agreement between 1D and 2D are excellent. Figure D7 makes the same comparison with run m43 that employed face-centered velocities and a tensorial Q. Some amount of phase shift is noticeable. However, for the 2D case, the near axis and the forty-five degree results are in close agreement, indicating good sphericity and the relative absence of noise. It is for this reason and the reduced presence of checkerboarding that we recommend face-centered velocities and a monotonic tensorial Q for calculating reactive flow at this point of code and model development.

Code Anomaly

Some spherical 1D problems were run using the code's metric option (curved zone faces are used in this option). Late in time, an angular asymmetry was observed. Furthermore, pressure spikes were observed in some of the calculations. This is in addition to the checkerboarding that has already been discussed. Causes for these anomalies were not pursued in the context of this work.

IV. Reactive Flow and Programmed Burn

The application described earlier was calculated using reactive flow in run m83 (set up like run m23) and was compared to a run that used programmed lighting augmented with beta burn (run m82). Figure E1 shows the positions of the shock that result from reactive flow and the predicted shock positions using programmed lighting (shortest optical paths resident in the explosive) at the same times. No corrections for shadowing (burn along

inert surfaces) were made in the programmed burn. Reactive flow clearly lags in time for reasons elaborated upon above. Except for this timing difference the two treatments give equally spherical results early in time; however, shadow velocities that are inherent in the reactive flow model increase this lag and induce changes of shape in the shock front compared to that predicted by programmed burn. Possible shadow corrections in programmed burn for lighting paths that are tangent to the sphere were not considered here for reasons of lack of data for such a high value of curvature.

Figure E2 shows a comparison of shock locations between programmed burn and reactive flow in the nearly asymptotic region well beyond the plastic sphere. The pseudo color plot is representative of the pressures at t = 7.0 μs. Figure E3 shows the effect of calculating the shock propagation with programmed burn that is assisted by beta burn. It is also seen to grow in a manner similar to that observed in the reactive flow calculations. The pseudo color plot shows the pressure at time t = 6.8 μs. Comparison with the previous plot shows considerable similarity between the result of the reactive flow calculation and the programmed burn calculation in terms of pressure levels and overall structure of the Mach stem region. In the reactive flow problem, however, the pressures are more uniformly high along the shock front than is the case in the programmed burn. Figure E4 compares shock positions calculated with reactive flow and beta burn-assisted programmed burn. The pseudo color plot shows pressures from the reactive flow calculation at t = 7.0 μs. It is apparent that the reactive flow produces a flatter shock front and that the Mach stem region is larger than for the programmed burn. A slightly faster rate of travel of the Mach stem calculated with reactive flow as compared to programmed burn with beta burn is also noticeable. While these differences are small, they are viewed as significant from a design standpoint when reflected shocks in burning high explosive are important.

Conclusions

Comparing geometry effects such as planar versus cylindrically and spherically expanding flow shows that asymptotic shock propagation speeds and maximum pressures are nearly the same in all geometries. The main differences are the slower propagation rate and the somewhat lower pressures during the early stages in divergent flow as well as the pulse shapes. A useful measure of the thickness of this ignition region in spherical coordinates is that it requires about 5 μs for the shock front to reach 99% of the asymptotic velocity or a radius of about 4.5 cm for LX-14. This result is consistent with an analytic theory in spherically divergent geometry. A preliminary calculation for LX-17 showed a similar result except that 26 μs were required for the shock front to reach 99% of the asymptotic speed.

A design problem that generates a Mach stem was calculated using reactive flow and compared to the results obtained using programmed burn augmented by beta burn. The differences were found to be small but significant in that the reactive flow produced a flatter shock front with more uniformly high pressures and exhibited a more extensively developed Mach stem which traveled slightly faster. It is suggested that this can have an important effect on designs that involve shock reflections in burning high explosive.

Zoning

It was found that zoning has to be carefully controlled. 1D problems calculated on a 2D mesh (spherical expansion on a stationary square mesh) compare well to the same problem run on a 1D mesh with comparable zoning. In 1D, zone refinement tends to speed up the shock, but refinement beyond 160 zones/cm produces no major change in the answers except that severe overshoots develop after some time at the leading edge of the shock which may be the result of boundary condition problems (see below).

In 2D, these overshoots appear to lead to "checkerboarding." "Checkerboarding" is a noise phenomenon that appears to be nearly harmless to the shock propagation rate and pressure levels of the main shock. Checkerboarding is the occurrence of alternately spaced high pressure zones at or slightly ahead of the leading edge of the shock. The location of this checkerboarding is affected by the choice of velocity differencing schemes. Face-centered velocities give checkerboarding near the axis in front of the shock. Corner-centered velocities (both the usual corner-centered velocities as well as the ALE treatment applied to the same stationary Eulerian mesh) give diagonally linked chains near the forty-five degree line. Another form of checkerboarding manifests itself in the appearance of single high-pressure zones or sometimes a few closely spaced high-pressures zones that wander through the mesh near the shock front when face-centered velocities are used. Because of the appearance of these zones on color plots of the pressure, we have dubbed this phenomenon "ruby-solitaire" checkerboarding.

Artificial Viscosity

Artificial viscosity (Q) has only a limited effect on the results. Tensorial, monotonic Q with face-centered velocities smoothes all checkerboarding and slightly retards the velocities (bringing them in closer coincidence with 1D results) compared to the same problem run with scalar Q. Tensorial Q run with corner-centered velocities accentuates the checkerboarding compared to scalar Q.

Anomalous Code Behavior

Anomalous code behavior was limited to checkerboarding (including solitaires) and the apparently associated overshoots of pressure pulses in 2D. If the zoning is too fine, a slight change in the evolution of the shock speed in spherically divergent systems is noted. The exacerbation of "checkerboarding" and overshoots when using corner-centered velocities was not expected. In 1D, spherical zoning that was too fine seemed to lead to overshoots. This may simply be the enhanced result of imperfect boundary conditions.

How to Run the Code

We find that a differencing scheme using face-centered velocities with a monotonic, tensorial Q gives the best, all-around results. Furthermore, for LX-14, zoning of 160 zones/cm produces consistent results as regards the shock formation and its propagation rate. Finer zoning changes the results only very slightly.

References

1. C.M. Tarver, J.O. Hallquist, L.M. Erickson, "Modeling Short Pulse Shock Initiation of Solid Explosives," *Proceedings for 8th Symposium (International) on Detonation,* Albuquerque, NM, July 15–19, 1985.

2. LeRoy G. Green and Edward James, Jr., "Radius of Curvature Effect on Detonation Velocity," Lawrence Radiation Laboratory, University of California, Livermore, California, in 4th Detonation Symposium (1965).

3. W.W. Wood and J.G. Kirkwood, "Diameter Effect in Condensed Explosives. The Relation between Velocity and Radius of Curvature of the Detonation Wave," *J. Chem. Phys.* **22**, 1920–24 (1954).

4. P.C. Souers, Ben Wu, L.C. Haselman, Jr., "Detonation Equation of State at LLNL, 1995," UCRL-ID-119262 Rev. 3, Lawrence Livermore National Laboratory, University of California, Livermore, California, February 1, 1996, pp. 8–11.

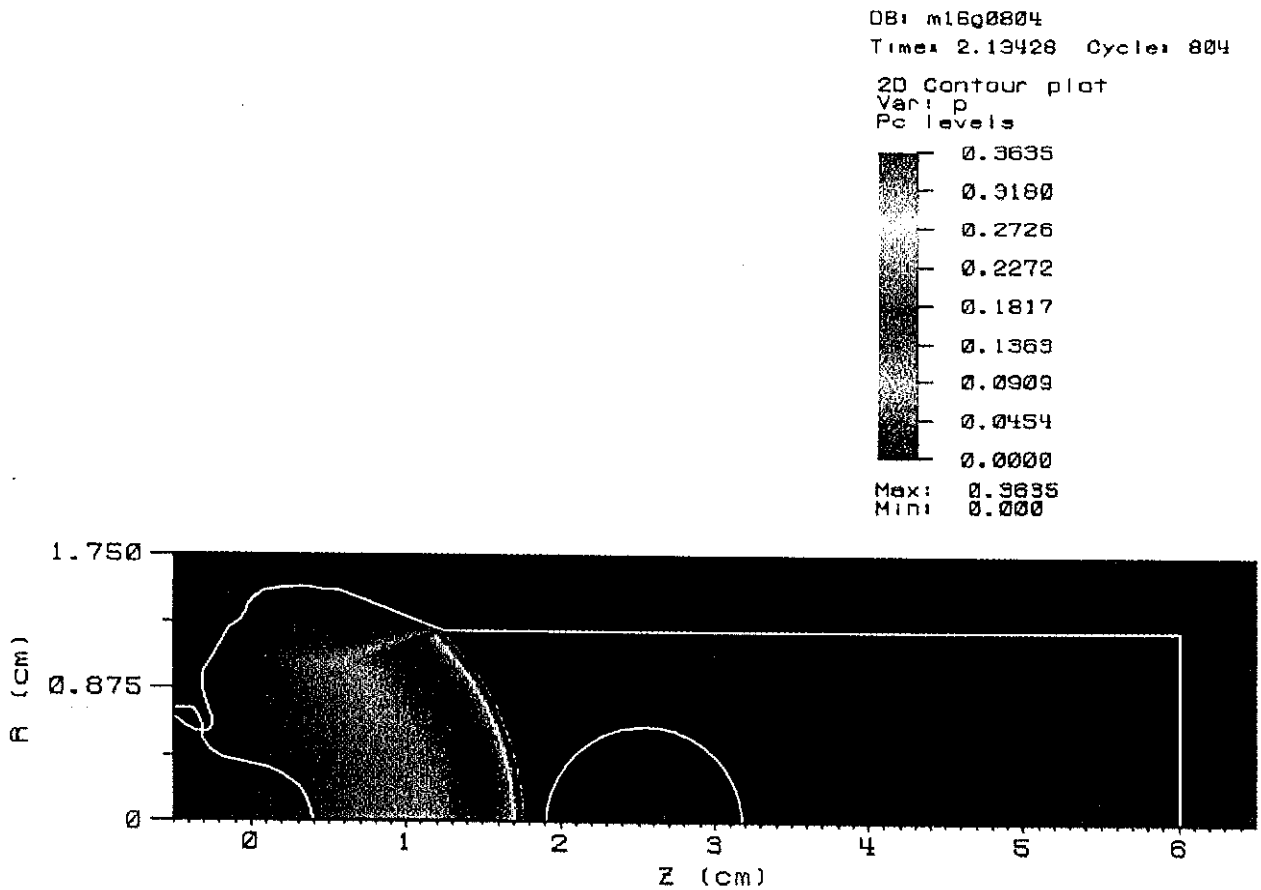

Figure A1. Color plot of pressures for application problem m16. The cylinder of high explosive is lit at z = 0 and r = 0 and burns around a plastic sphere (circle in the middle).

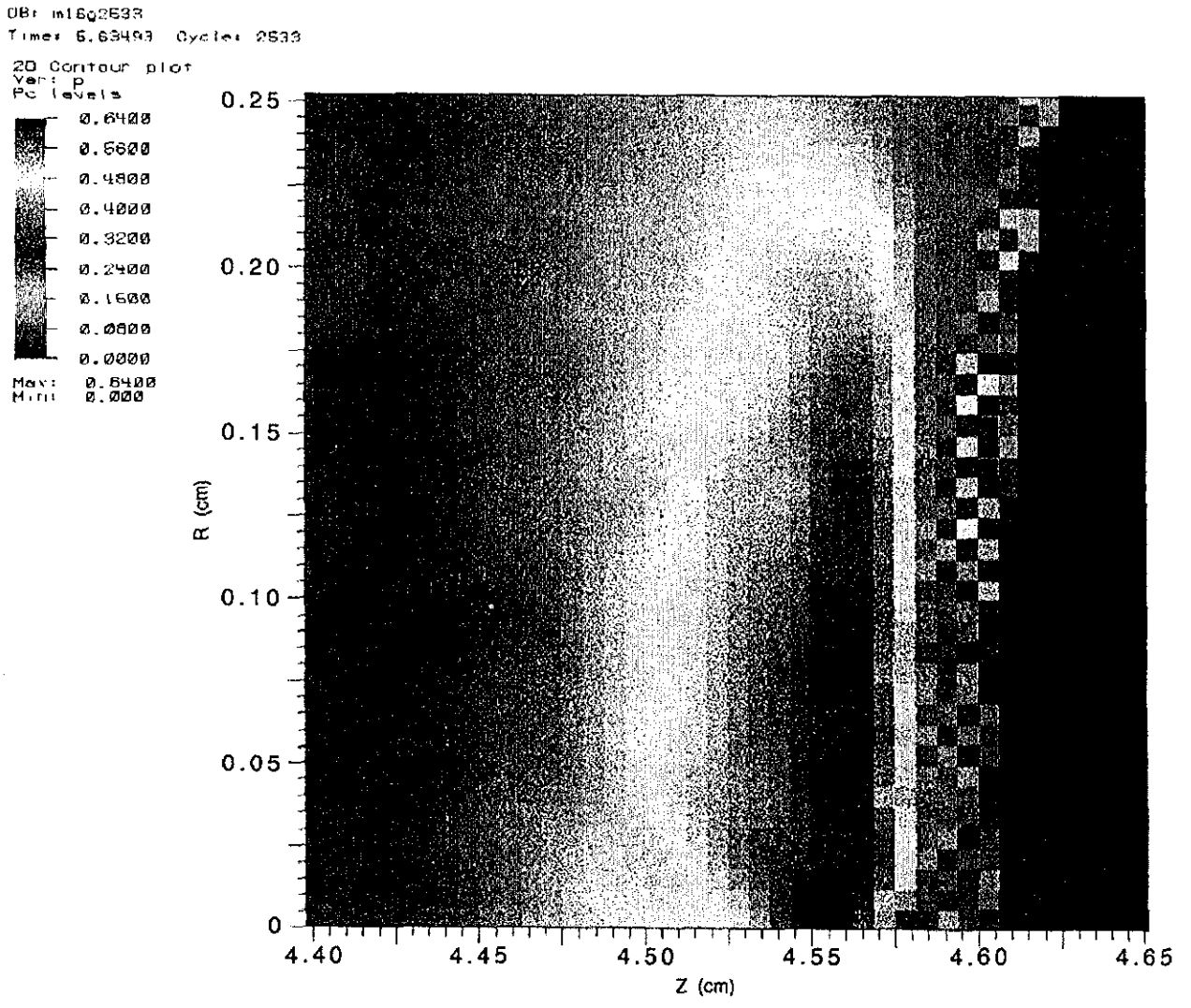

Figure A2. Color plot of pressures in the Mach stem region for run m16 (face-centered velocities, scalar Q). Checkerboarding ahead of the Mach stem and noise in the Mach stem region are clearly visible.

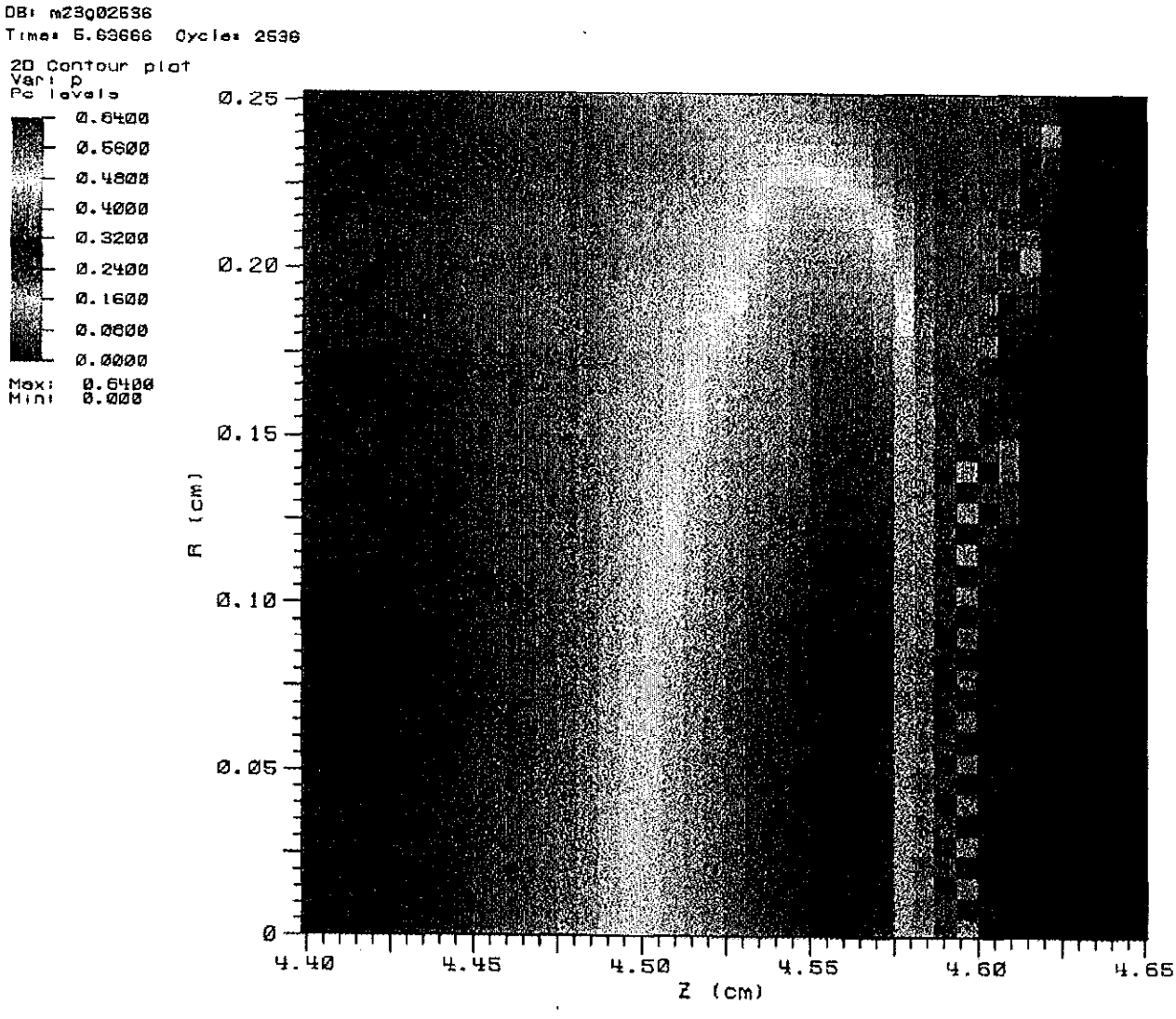

Figure A3. The Mach stem region smoothed by tensorial Q in run m23 (face-centered velocities, tensorial Q). Otherwise this run is identical to m16 (face-centered velocities, scalar Q, Fig. A2). A certain amount of undercutting of the backside of the Mach stem in run m16 has disappeared in this run.

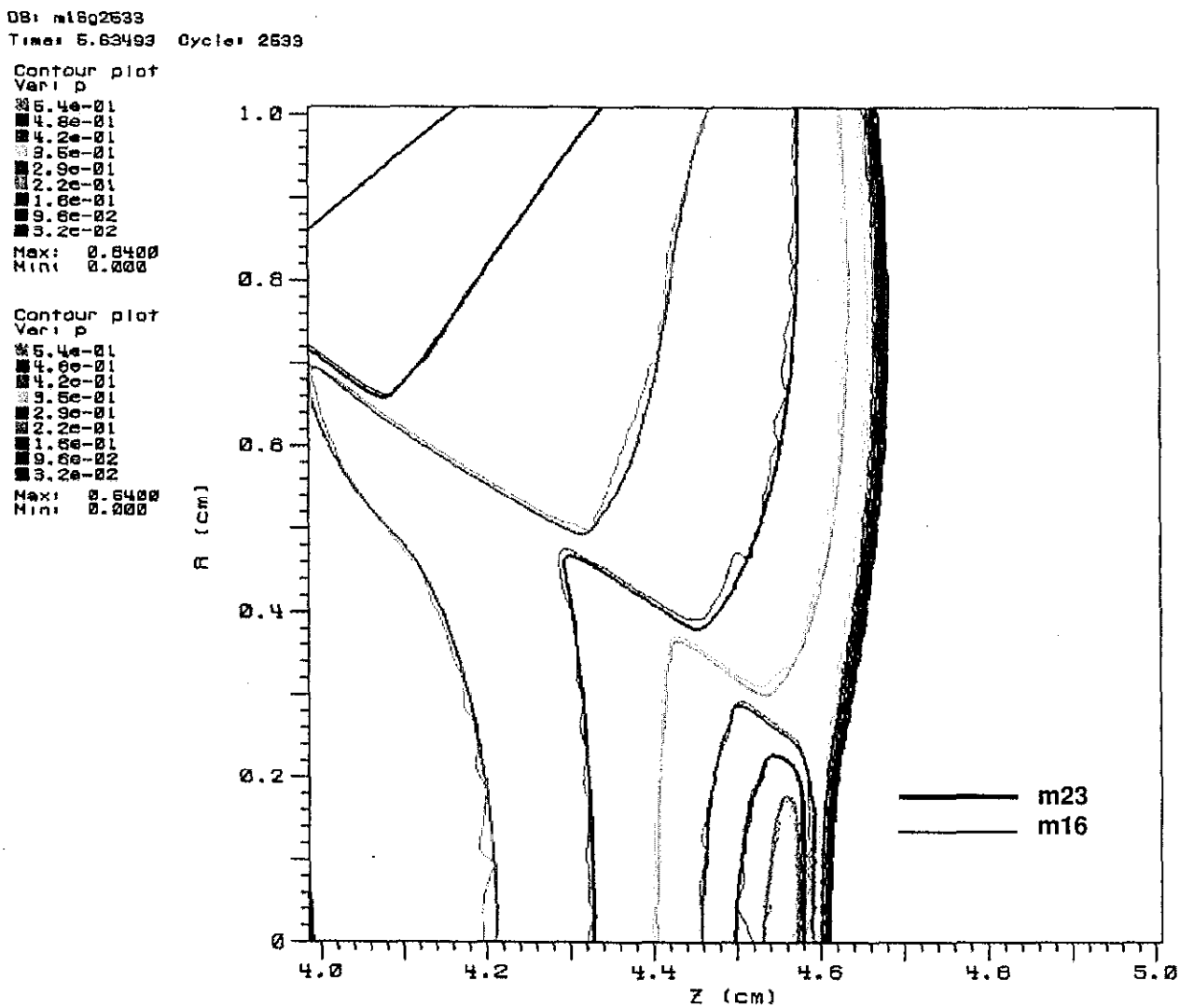

Figure A4. Contour overlay comparing runs m16 (scalar Q, light contours) and m23 (tensorial Q, heavy contours). Smoothing of noise seems to be the principal effect of tensorial Q near the axis for face-centered velocities.

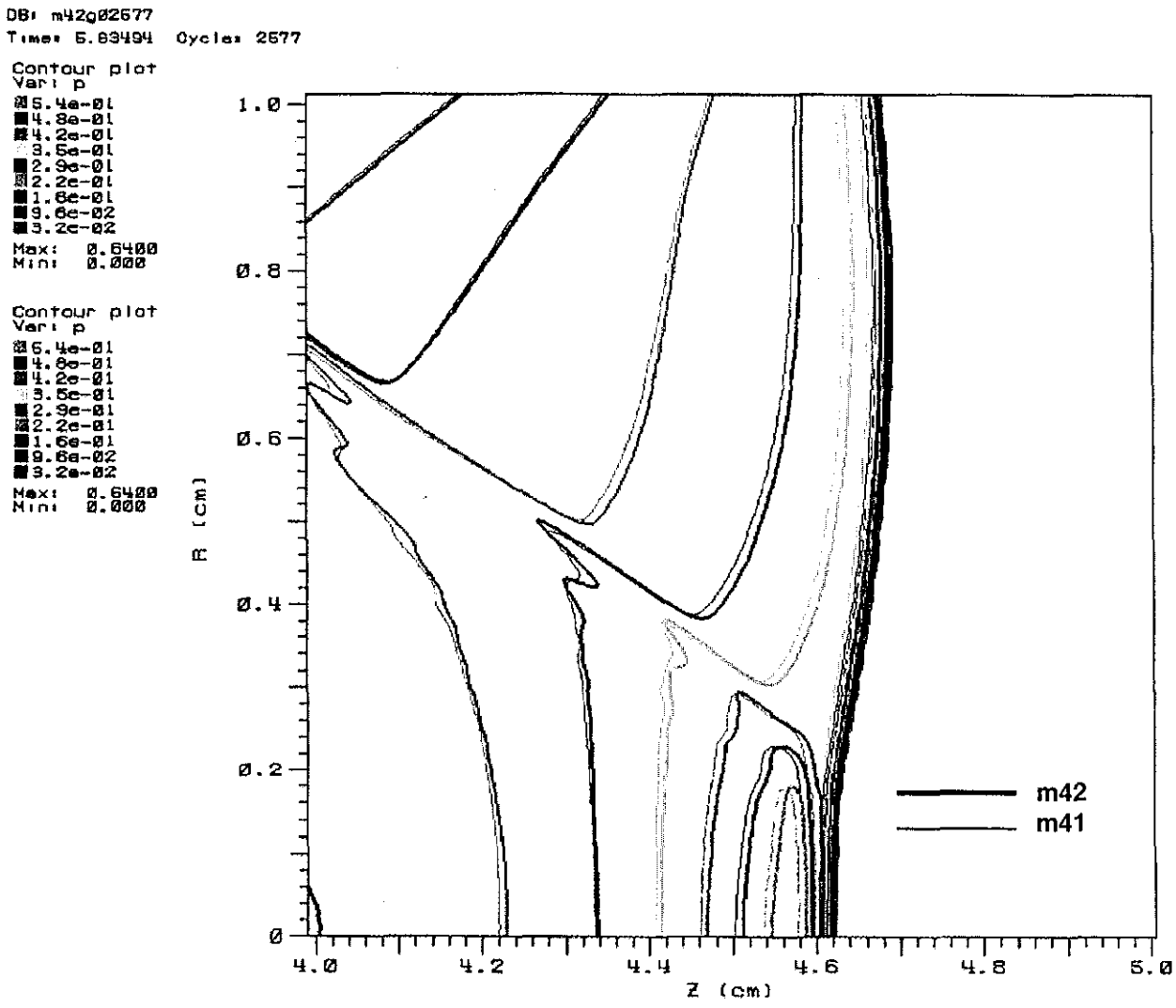

Figure A5. Comparison of the effect of scalar Q (run m41, light contours) versus tensorial Q (run m42, heavy contours) on the contours in the Mach stem region for corner centered velocities.

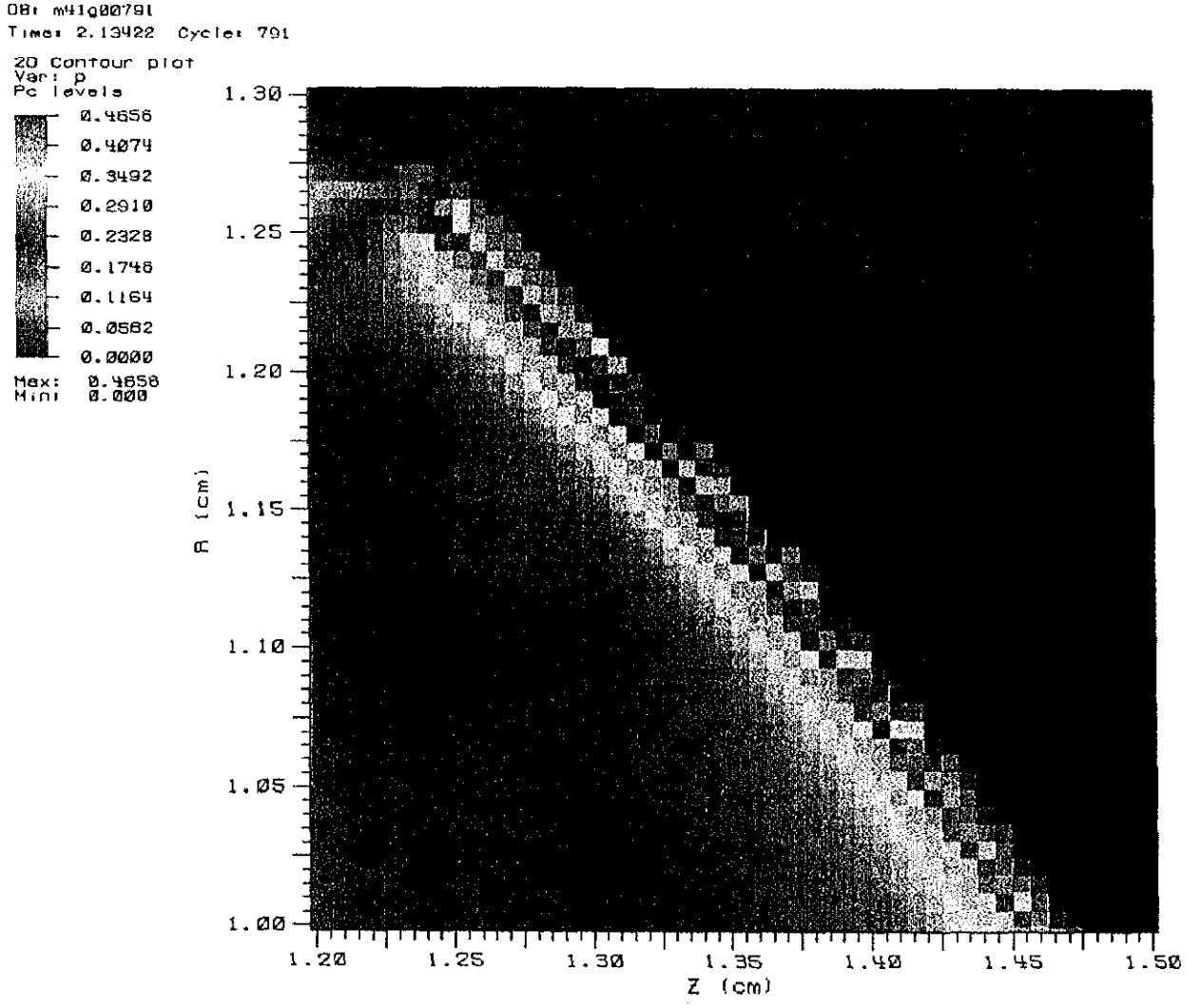

Figure A6. Checkerboarding chains near the 45° line for corner-centered velocities in run m41. The amplitude of the checkerboarding exceeds the pressures of the main pulse which are consistent with other calculations such as expanding spheres.

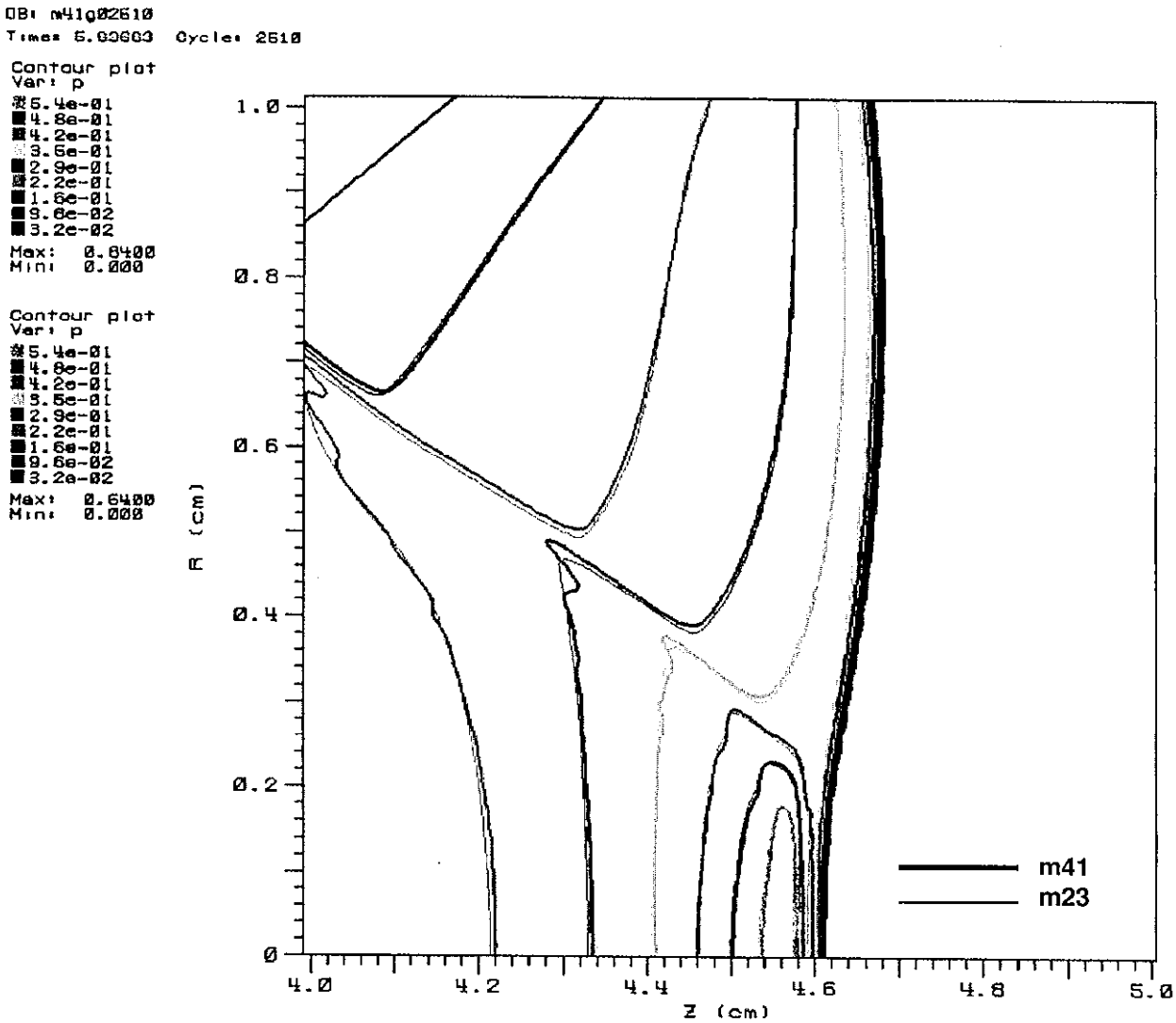

Figure A7. Comparison of pressure contours in the Mach stem region for face-centered velocities and a tensorial Q (run m23, light contours) and corner-centered velocities with a scalar Q (run m41, heavy contours). For run m41 diagonal checkerboarding is illustrated in Figure A6.

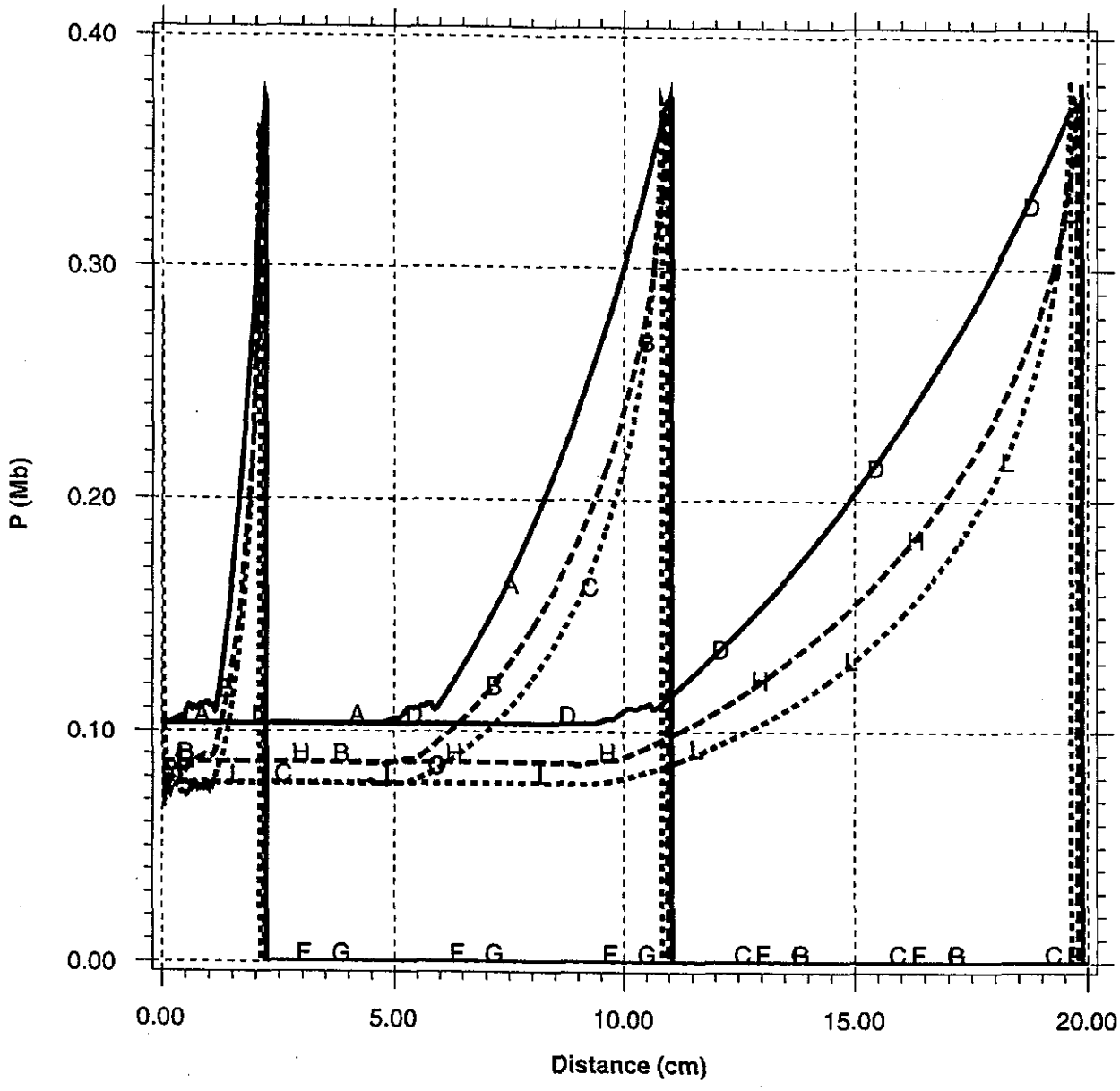

Figure B1. Snap shots of the pressure profiles at three different times for planar (run m38), cylindrical (run m39) and spherical (run m40) geometries. The solid lines are the planar problem, the dashed lines are the cylindrical problem and the dotted lines are for the spherical problem. Pulse broadening in time is very obvious.

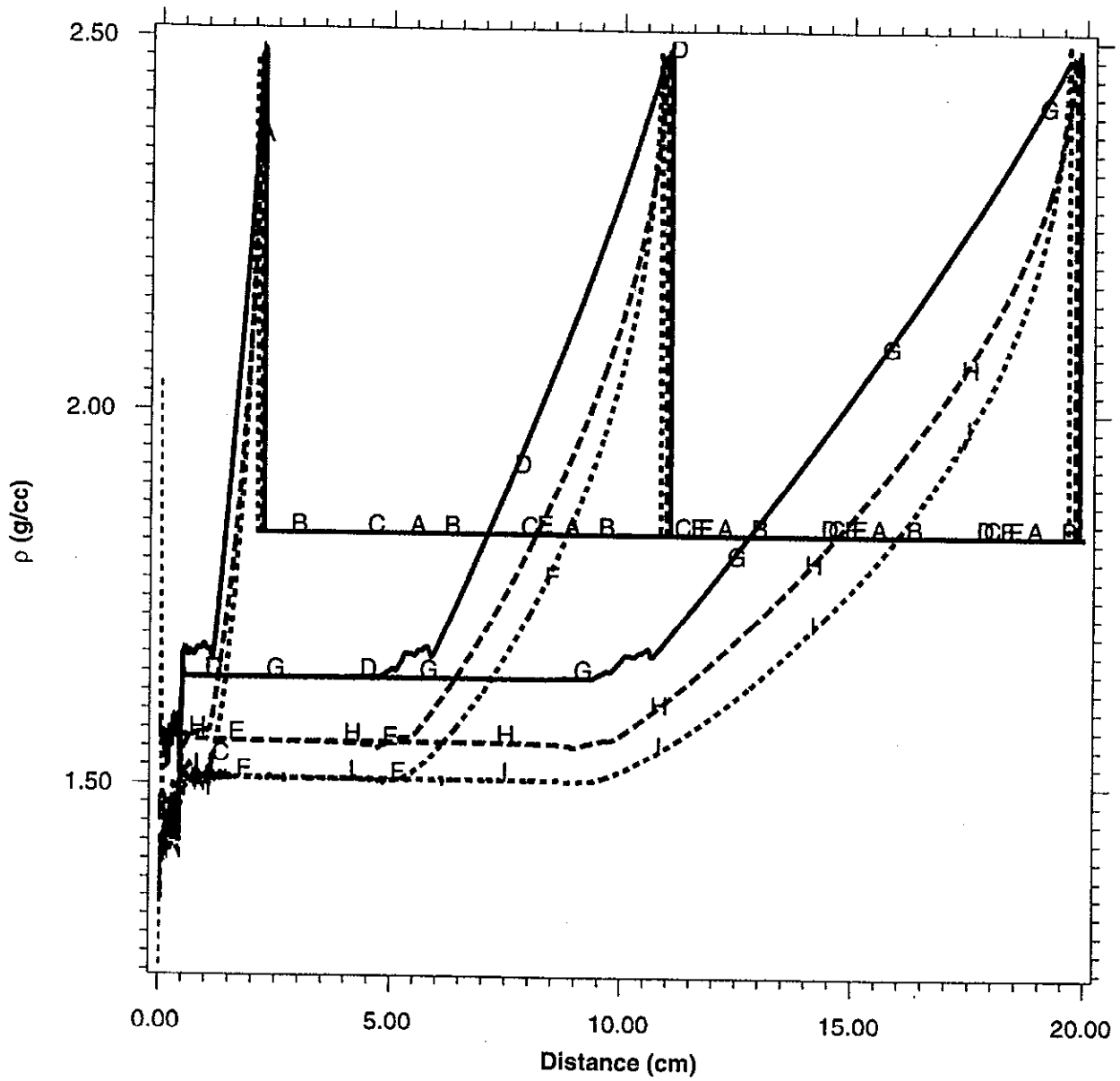

Figure B2. Density profiles for the pulses in Figure B1.

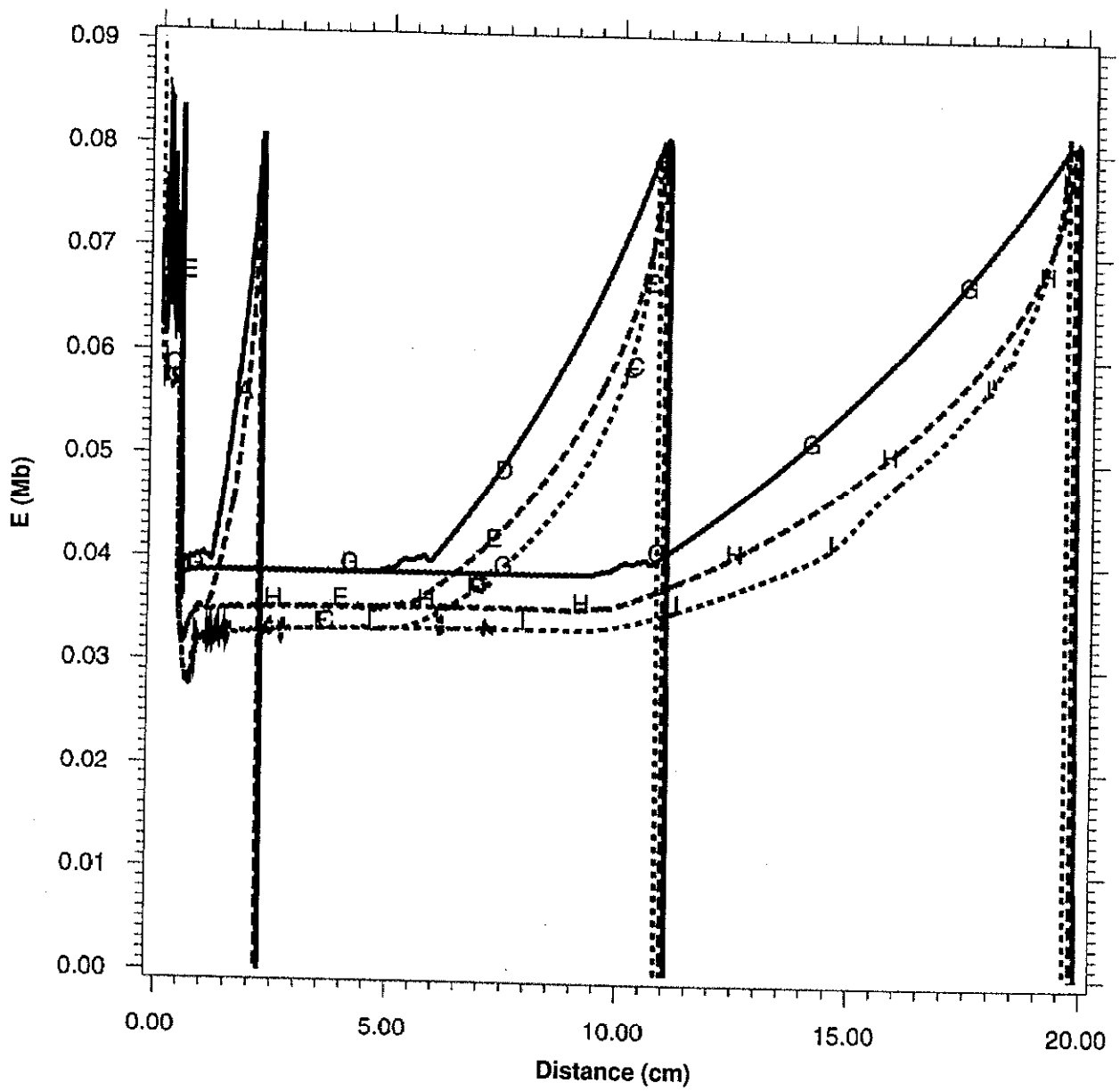

Figure B3. Energy profiles for the pressure pulses in Figure B1.

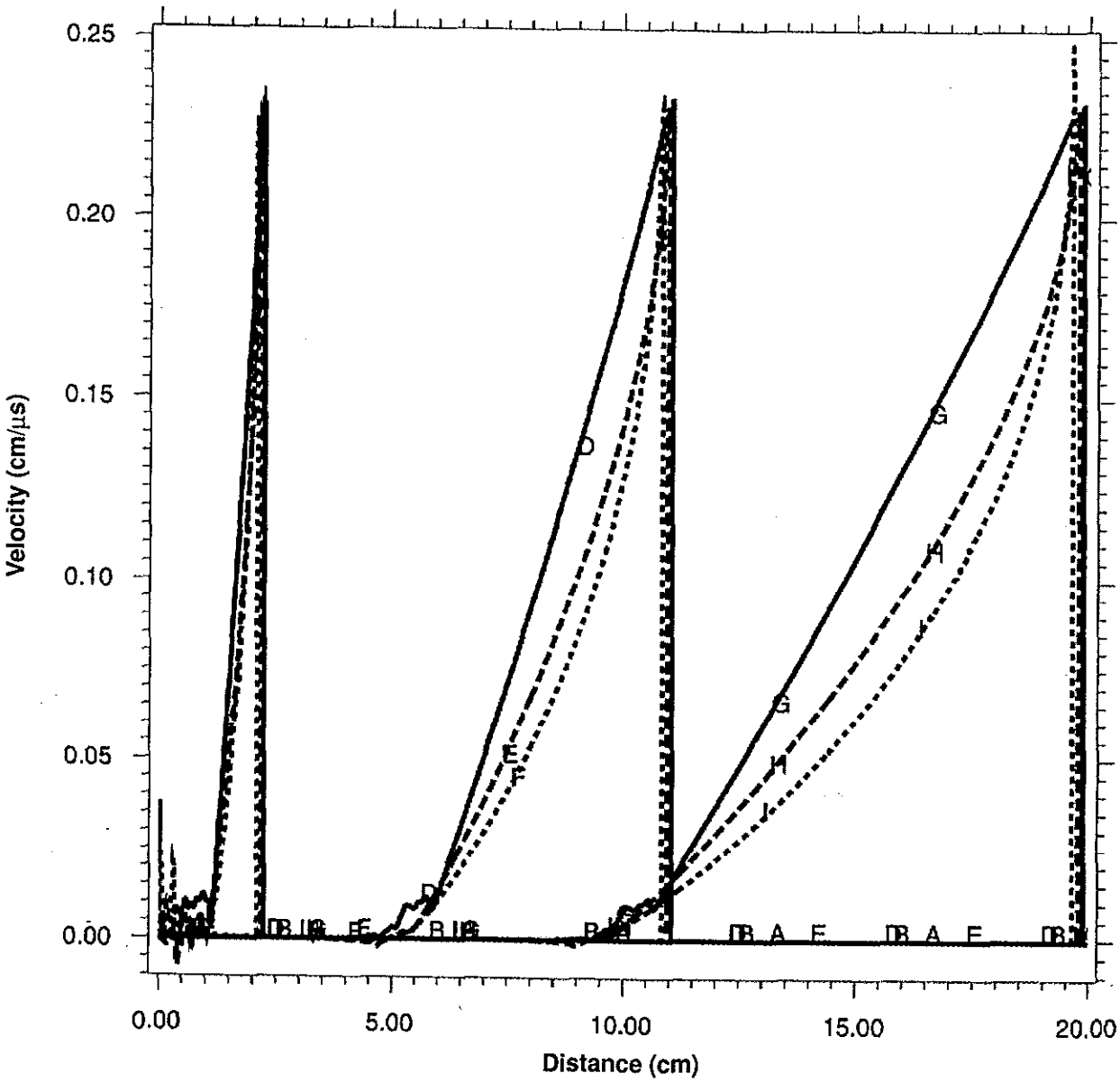

Figure B4. Velocity profiles for the pressure pulses in Figure B1.

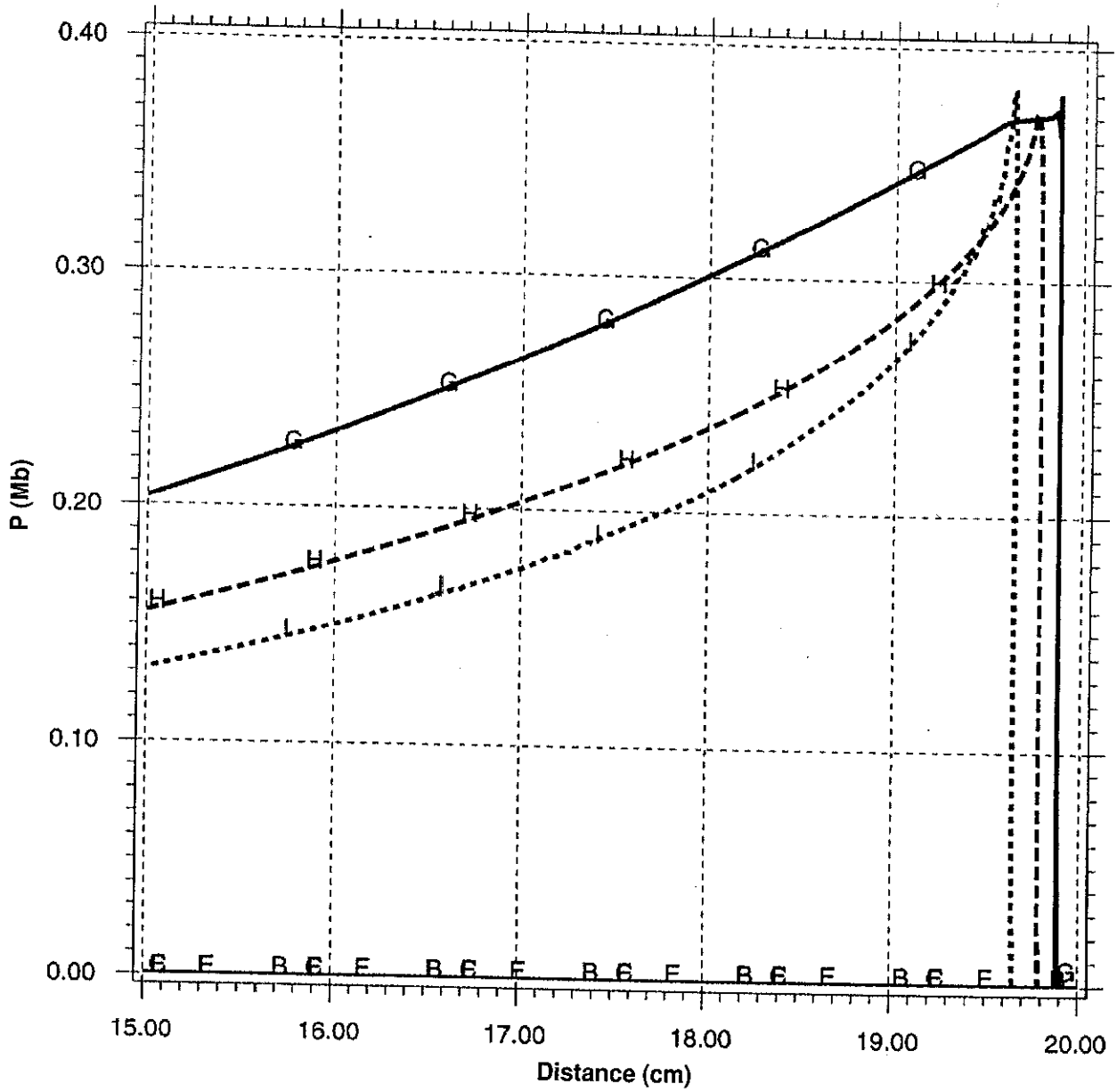

Figure B5. A close-up of the pressure pulses in Figure B1. The pulses for the cylindrical and spherical problems lag behind the planar one. The lag for the spherical case is greatest because of the higher divergence.

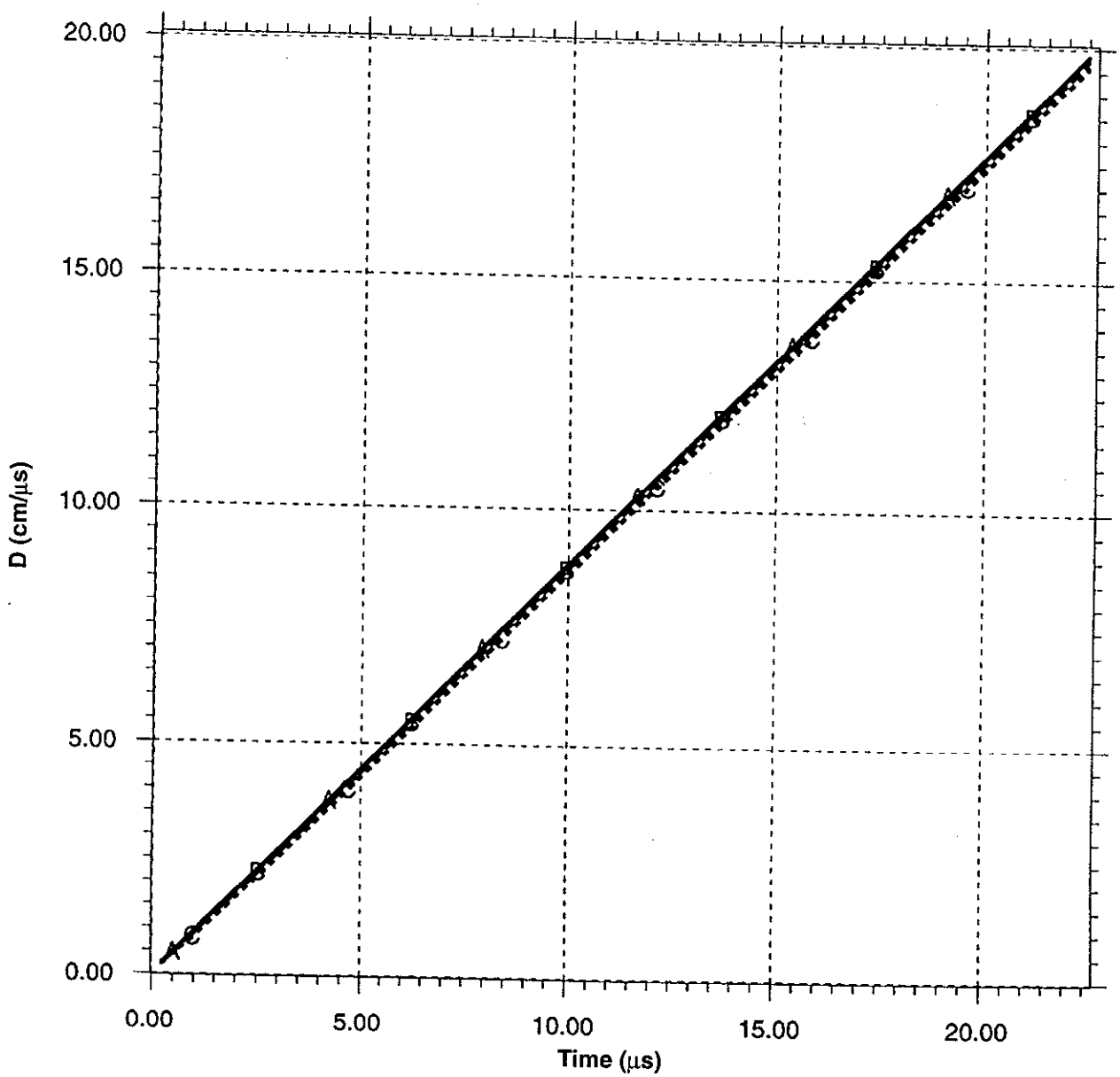

Figure B6. The shock positions versus time for the problems of Figure B1.

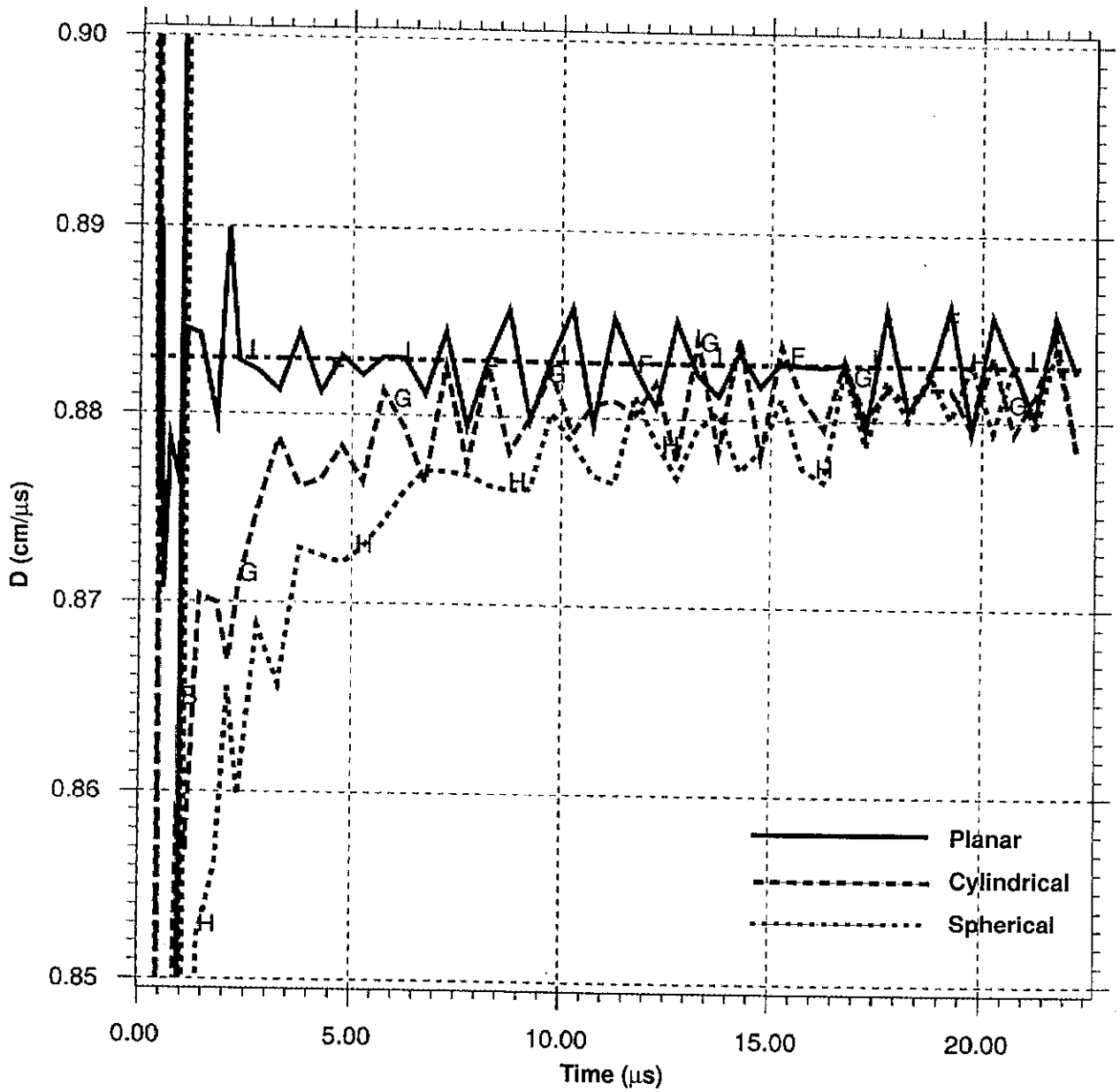

Figure B7. The shock speeds for the problems in Figure B1. The speeds are the simple derivatives of the lines in Figure B6. The horizontal straight line shows the theoretical, steady state shock speed of 0.883 cm/μs.

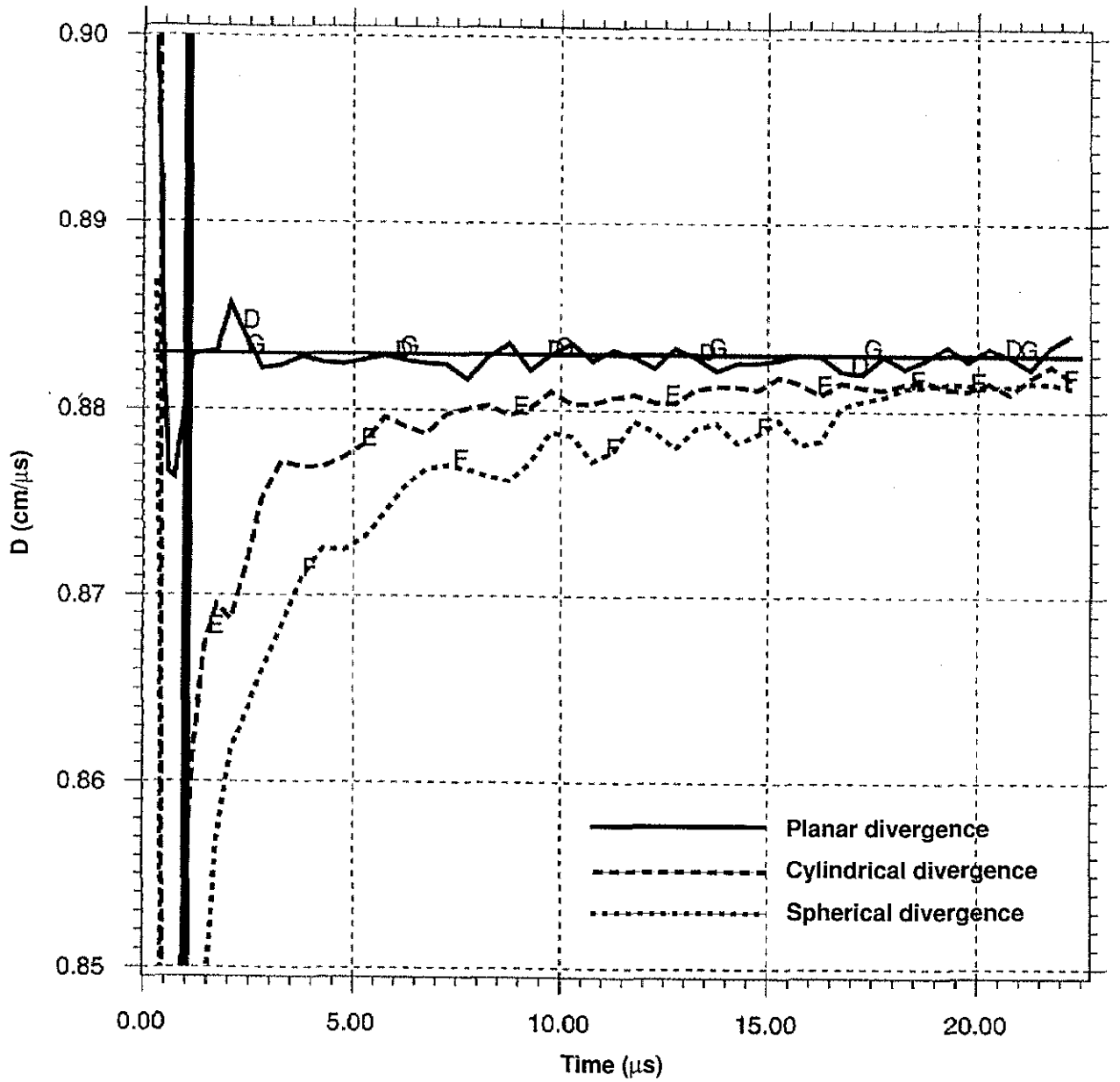

Figure B8. The shock speeds of Figure B7 smoothed. It is apparent that geometric divergence, both cylindrical and spherical, retard the early buildup of the shock speed. The horizontal line shows the theoretical shock speed of 0.883 cm/μs.

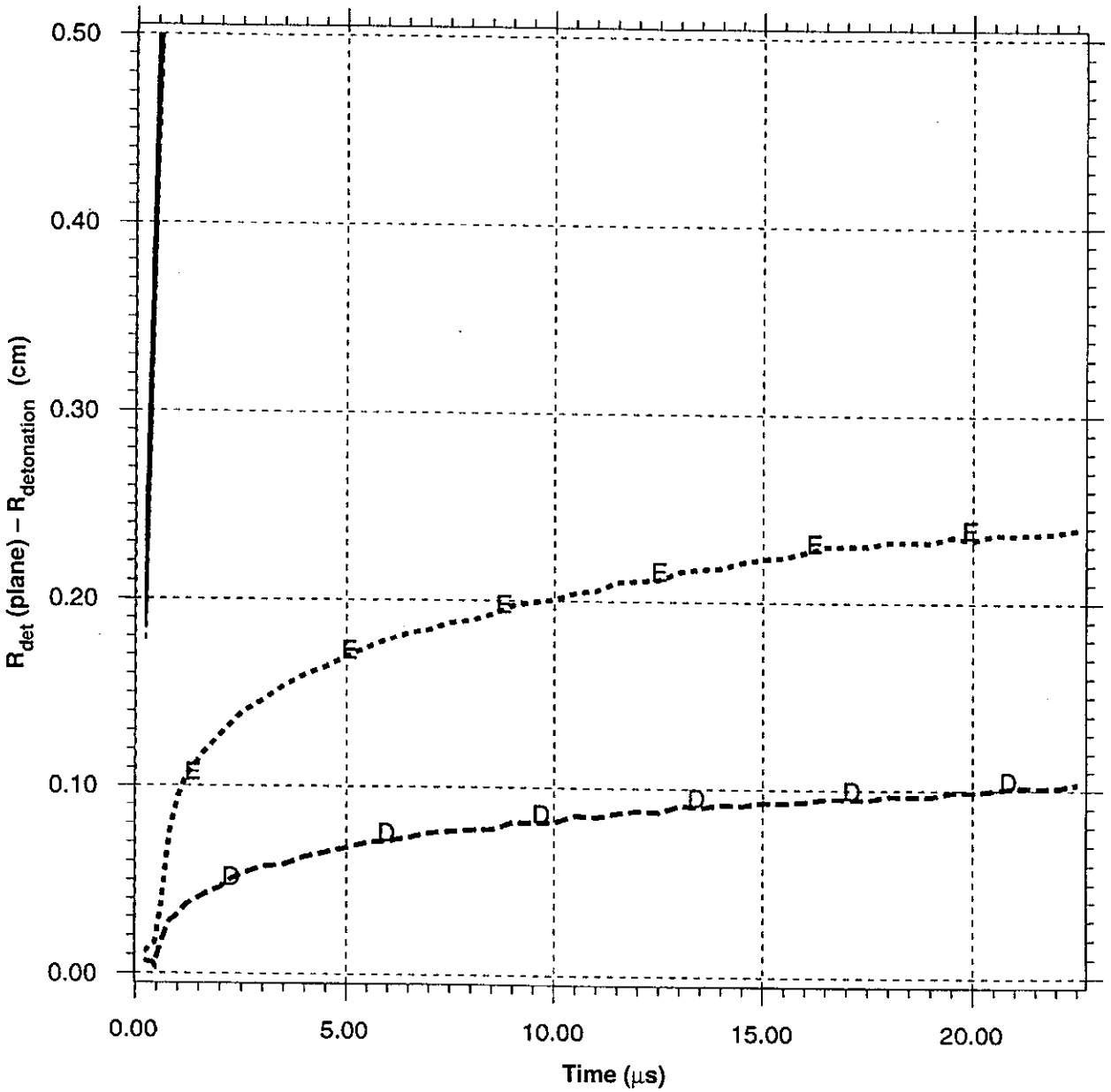

Figure B9. The difference in the shock positions of the problems in Figure B1. Run m38 serves as a reference run from which the other two are subtracted. It is apparent from this figure and from Figure B4 that the spherically divergent case (curve E) takes longest to establish its steady state propagation rate.

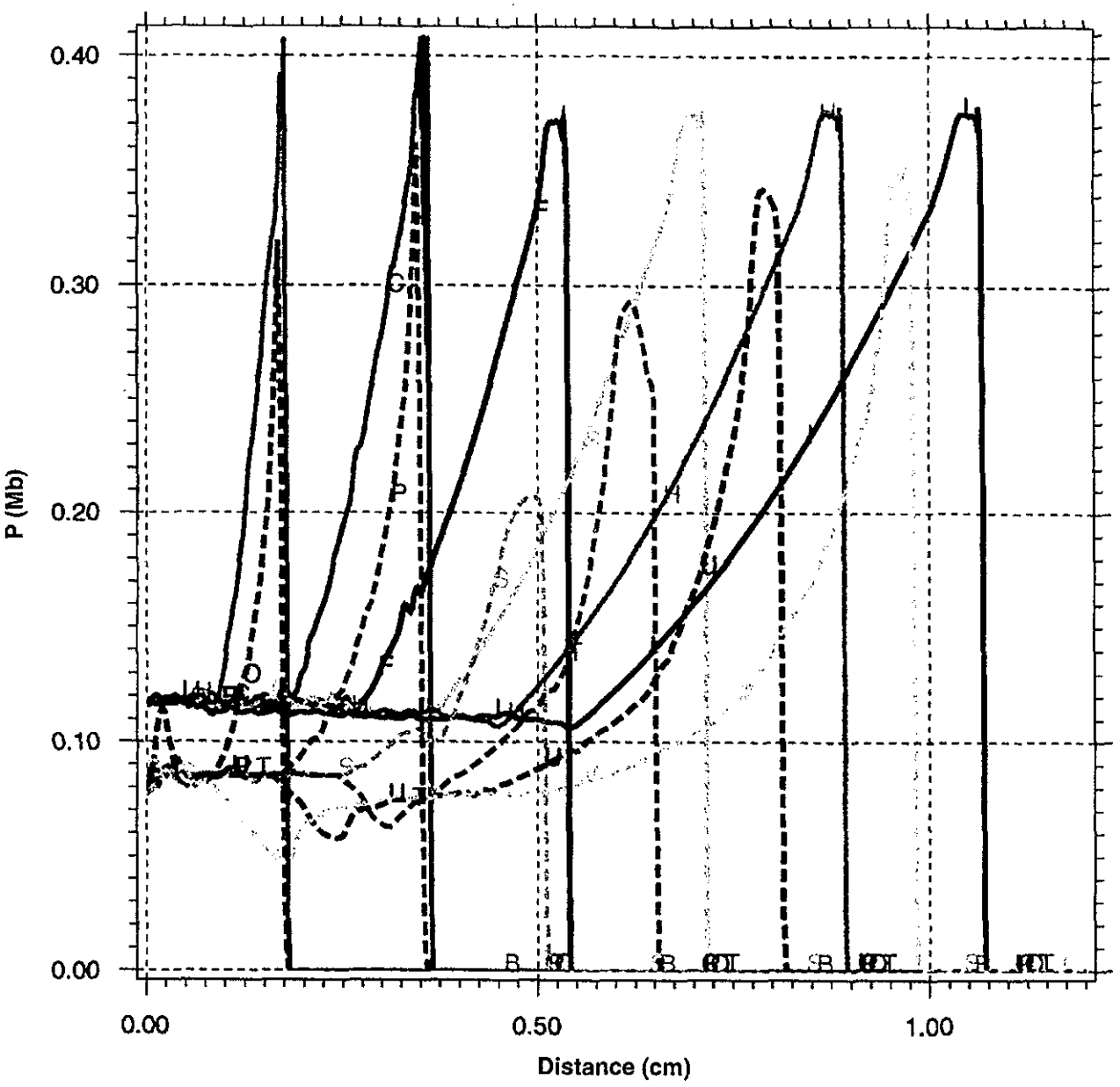

Figure B10. Pulse shapes for runs m50 (planar, solid lines) and m65 (spherically divergent, dashed lines) are compared every 0.2 μs. The discontinuity in pulse shapes from the programmed lighting portion (first 0.4 cm) to the reactive flow portion is apparent for the spherically divergent case. It is also clear that the narrowness of the pulses in spherical geometry reduces the available impulse. Furthermore, for spherical geometry the pulse height takes time (or reduced divergence) to build its amplitude even in the programmed burn region.

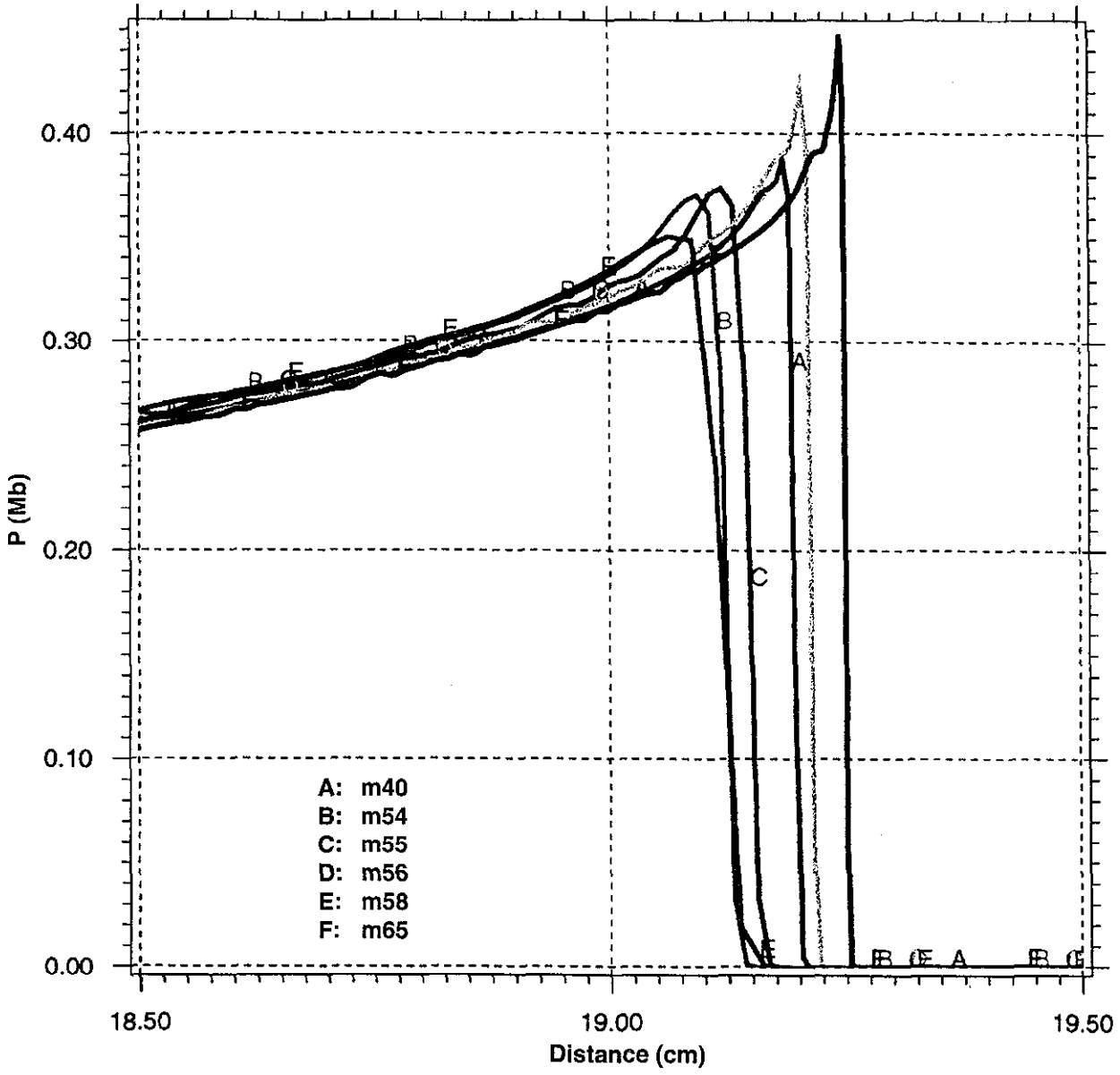

Figure C1. Close-up of the pressure profiles for spherically diverging problems m40, m54, m55, m56, m58 and m65 that differ only in zoning (see Table I). The finest zoning gives the most advanced pulse and the coarsest zoning gives the most retarded pulse. The finer zoning also is susceptible to overshoots as is seen for the pulse from problem m65. These overshoots appear to be persistent once they make their appearance. The Chapman-Jouget pressure for this high explosive is 0.381 Mb when density = 1.835 g/cc, E_0 = 0.101 e.u./cc, and the Haselman high CJ eos is used.

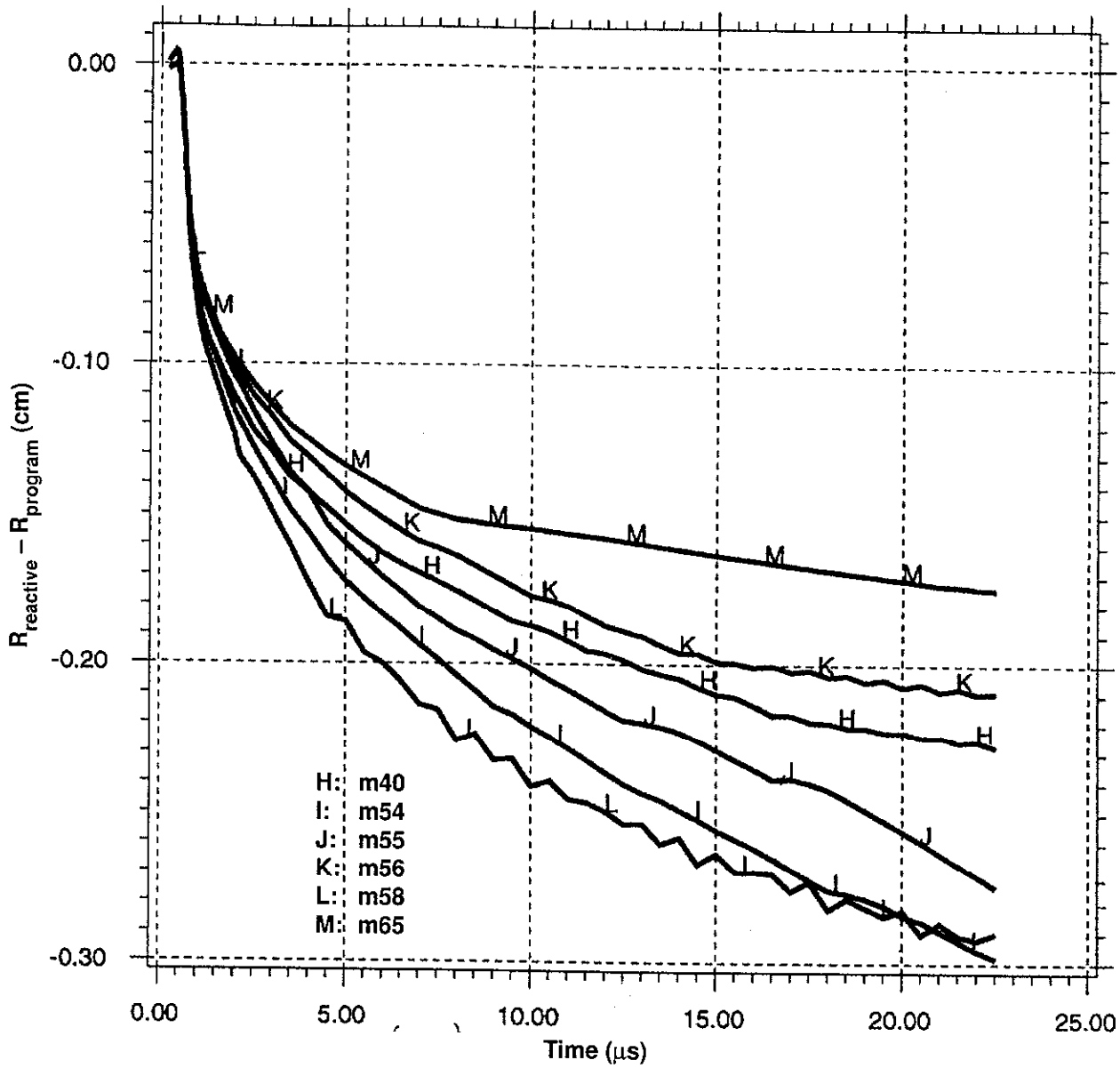

Figure C2. Differences in shock positions versus time for spherically diverging problems (m40, m54, m55, m56, m58 and m65) run on a spherical, metric mesh. The shock positions calculated from reactive flow are diminished from the programmed burn positions that would be achieved with a detonation speed of 0.883 cm/μs. The more finely zoned problems (curves H, K and M for runs m40, m56, and m65 respectively) show clear signs of tending towards an asymptote. The obviously linear portion of curve M (run m65) is associated with the existence of the overshoot on the pressure pulse which appears at a time of about 7 μs. The most coarsely zoned problem (m58) also produces the most noise (curve L) and lags behind the programmed burn the most.

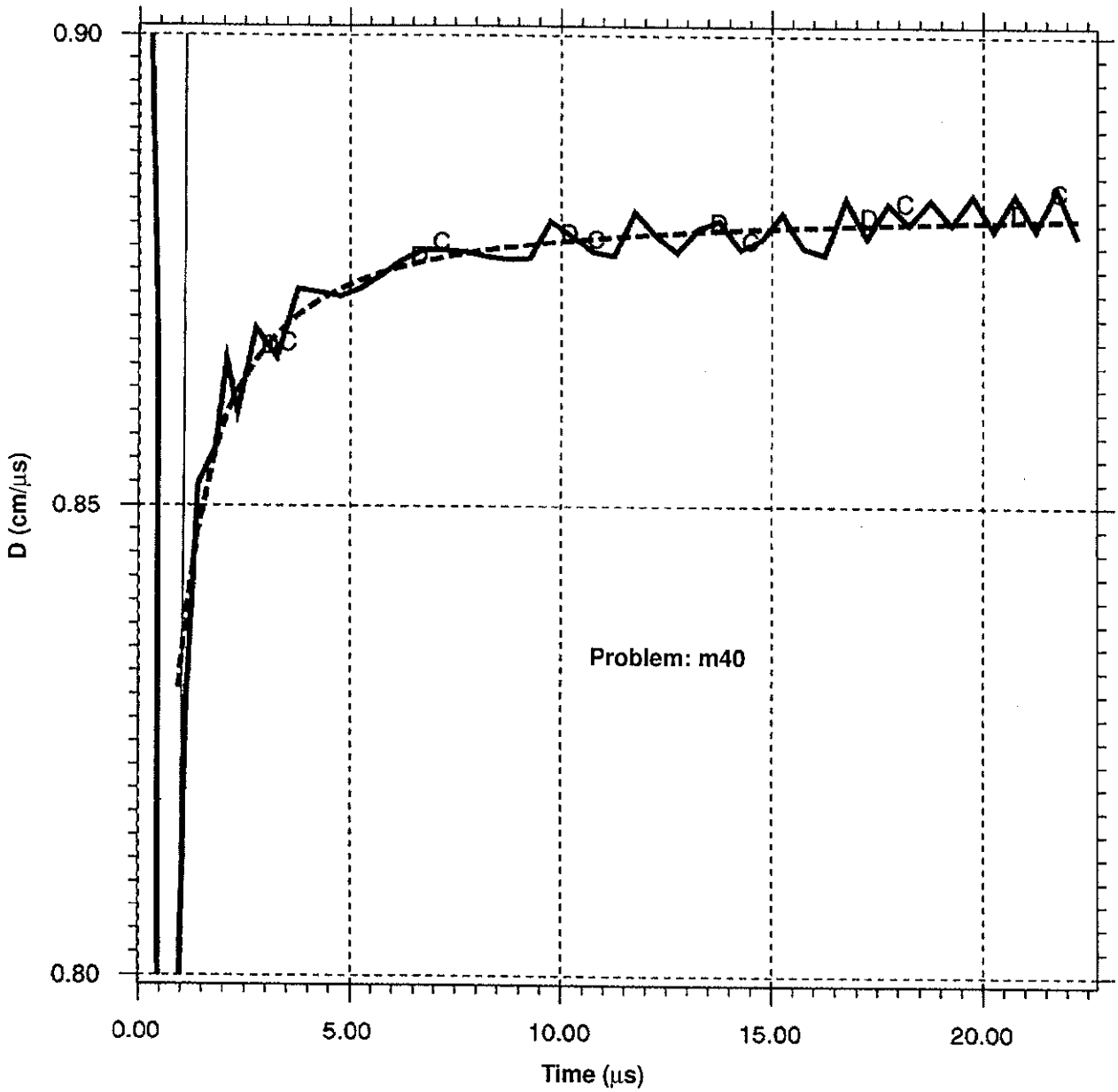

Figure C3. Numerical derivatives of the shock positions versus time for problem m40 and the analytic fit (dashed curve) of the theory. The fitting constants are given in Table III.

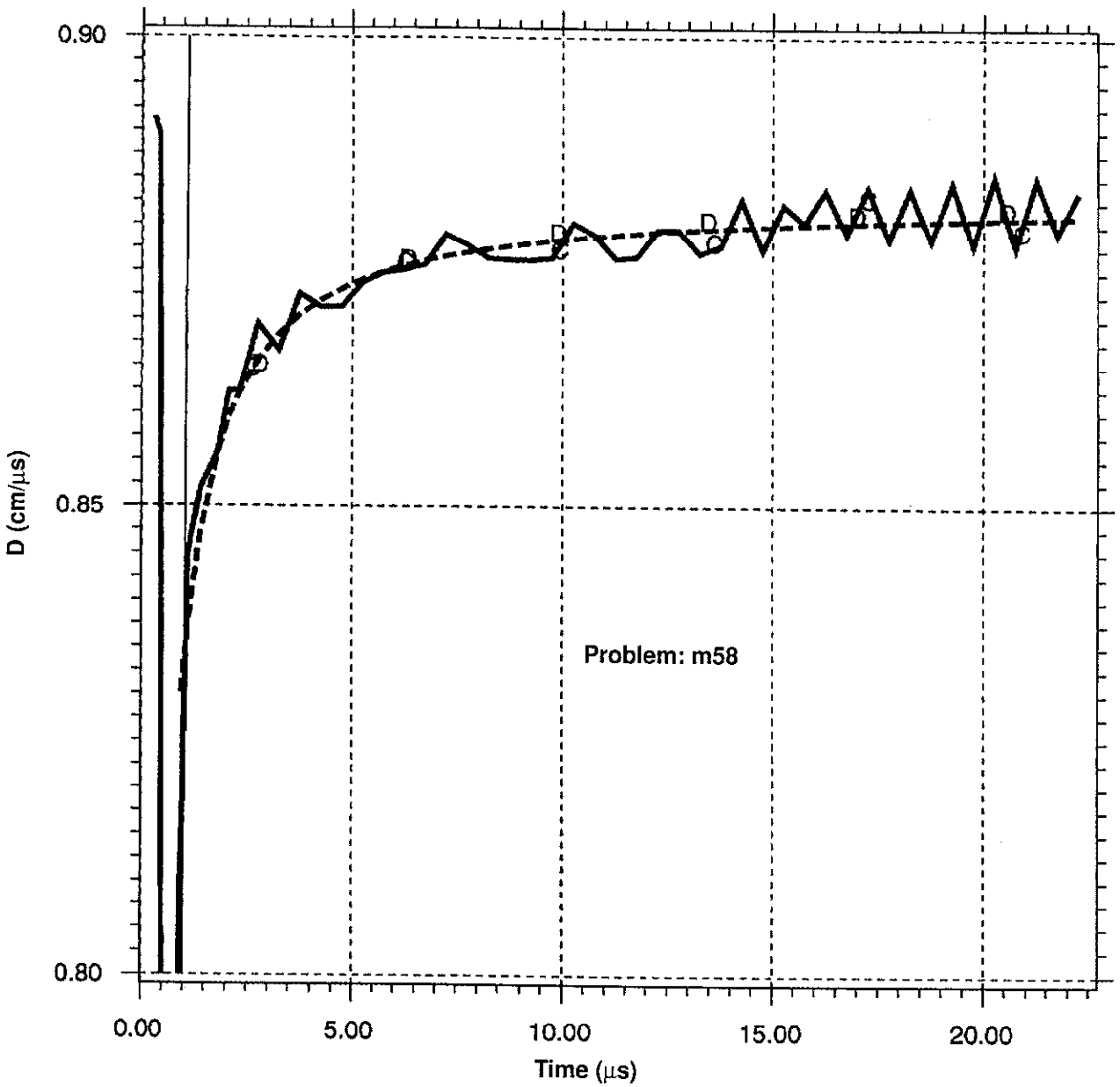

Figure C4. Numerical derivatives of the shock positions versus time for problem m58 and the analytic fit (dashed curve) of the theory. The fitting constants are given in Table III.

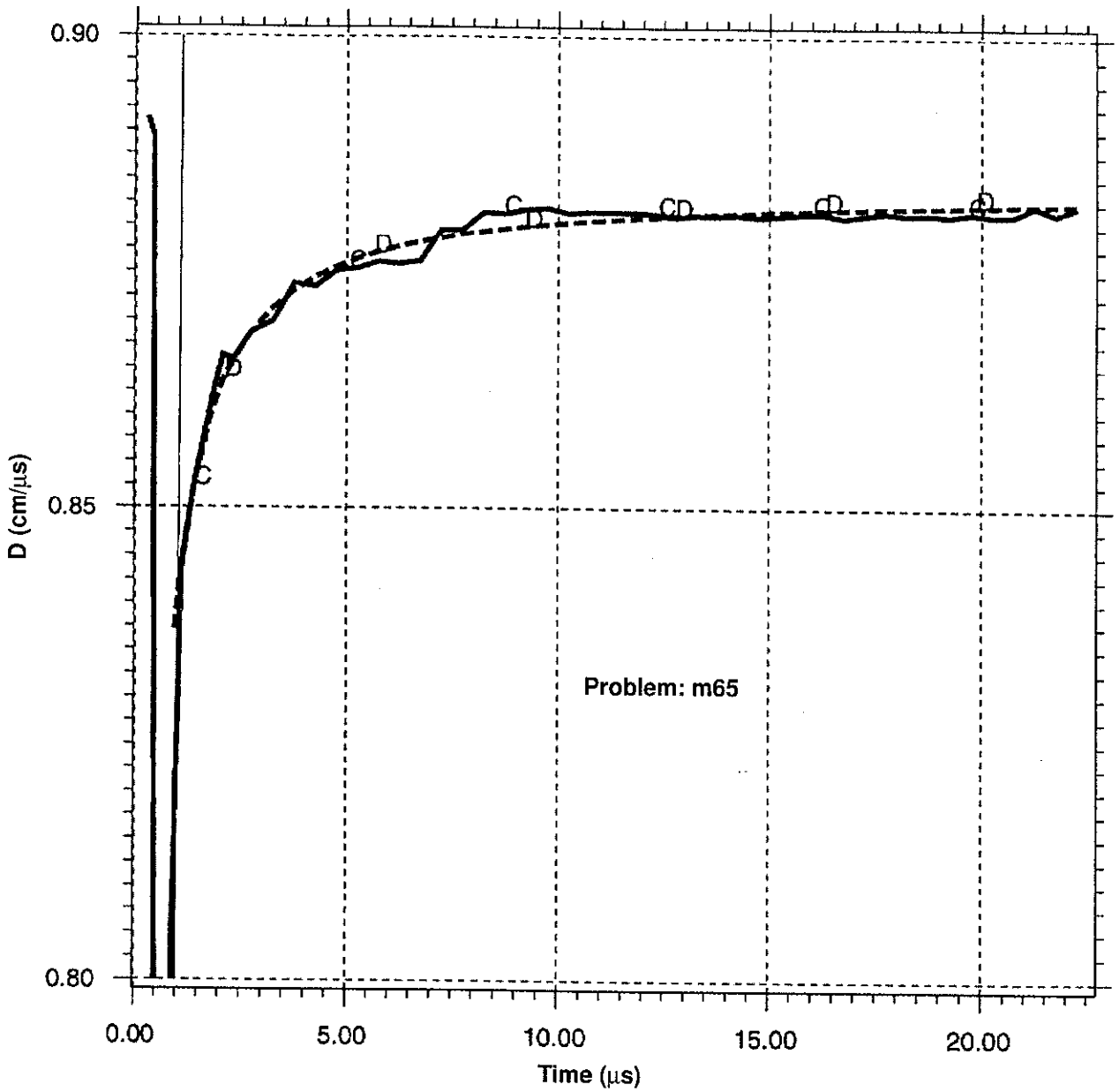

Figure C5. Numerical derivatives of the shock positions versus time for problem m65 and the analytic fit (dashed curve) of the theory. The fitting constants are given in Table III.

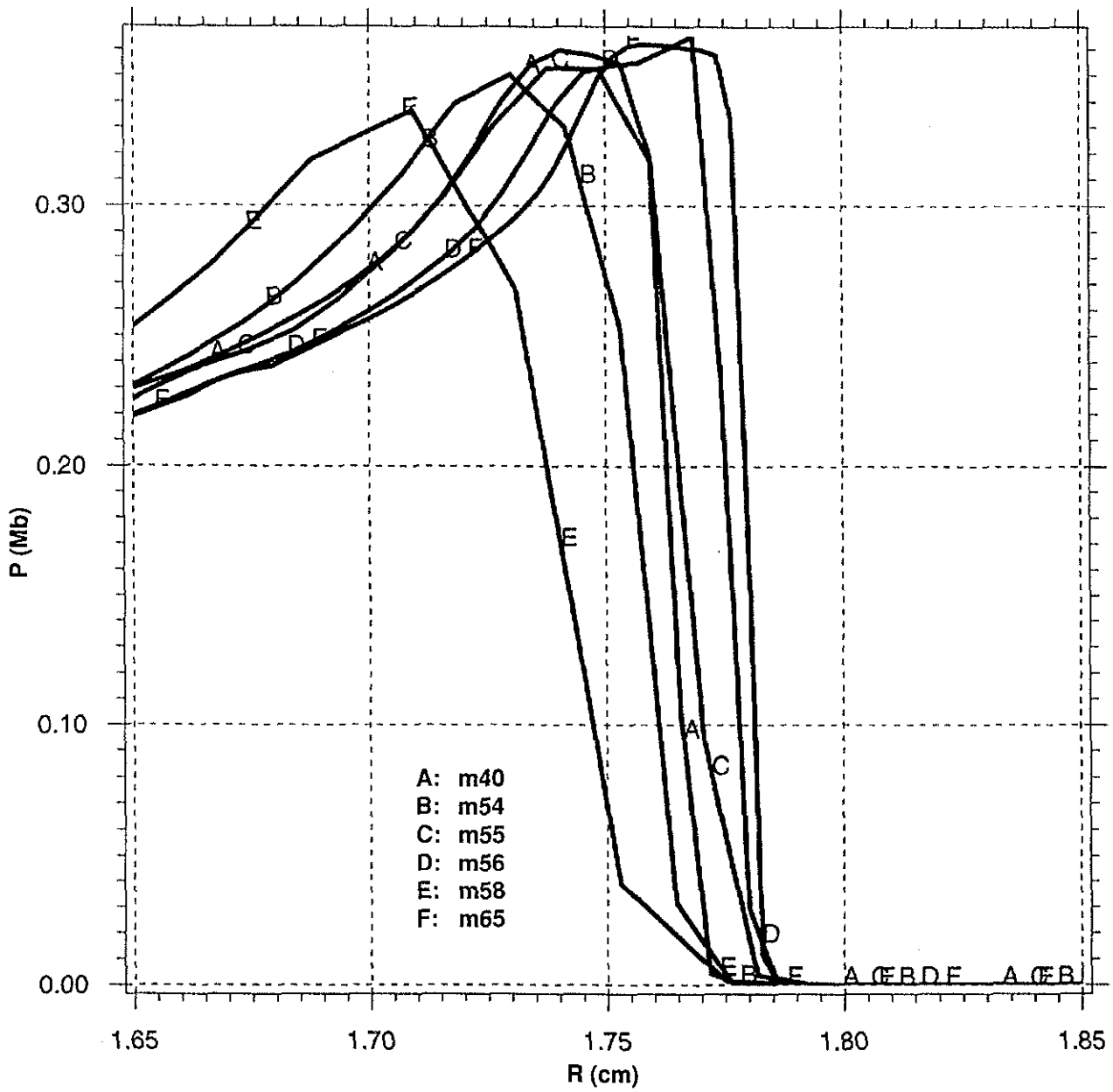

Figure D1. Pressure profiles for the 1D spherical runs in Figure C1 at the earlier time of about 2.132 μs. Apparently in 1D, finer zoning speeds up the shock front. Overshoots have not developed at this early time. See Table III for zoning information.

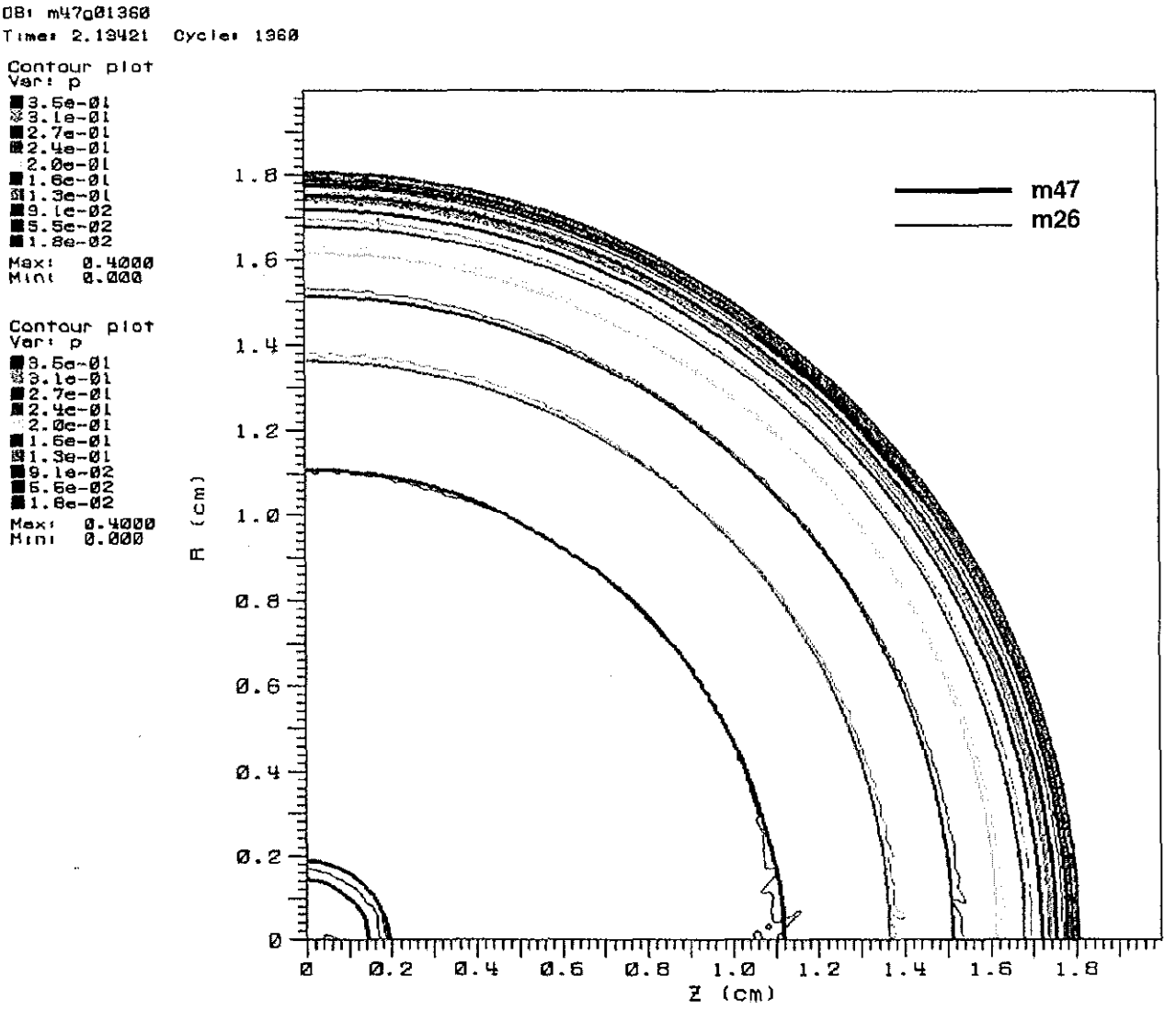

Figure D2. Overlay of pressure contours for run m26 (face-centered velocities, heavy contours) and run m47 (corner-centered velocities, light contours). Both runs use scalar Q. Checkerboarding for run m47 manifests itself as a smudged contour near the 45° line.

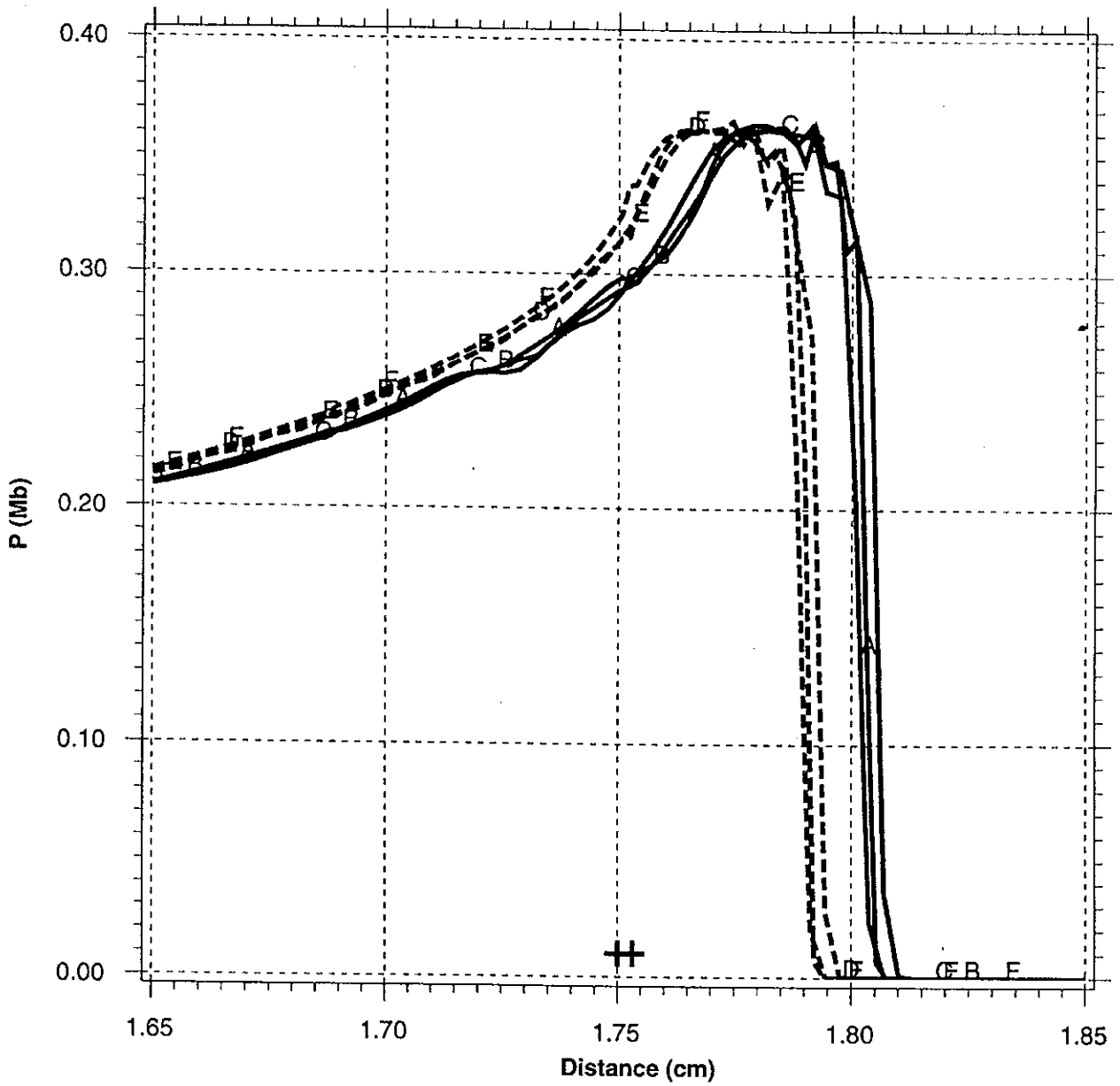

Figure D3. The effect of scalar and tensorial Q for face-centered velocities. Profile plots of pressures for problems m26 (scalar Q, solid lines) and m43 (tensorial Q, dashed lines) at a time of about 2.13 μs. The profiles are taken at about 3° and 87° and at 45°. The spacing between the two "plus-signs" indicates the length of the zone edges. The tendency to overshoot at the leading edge of the shock appears to be mitigated by the choice of face-centered velocities.

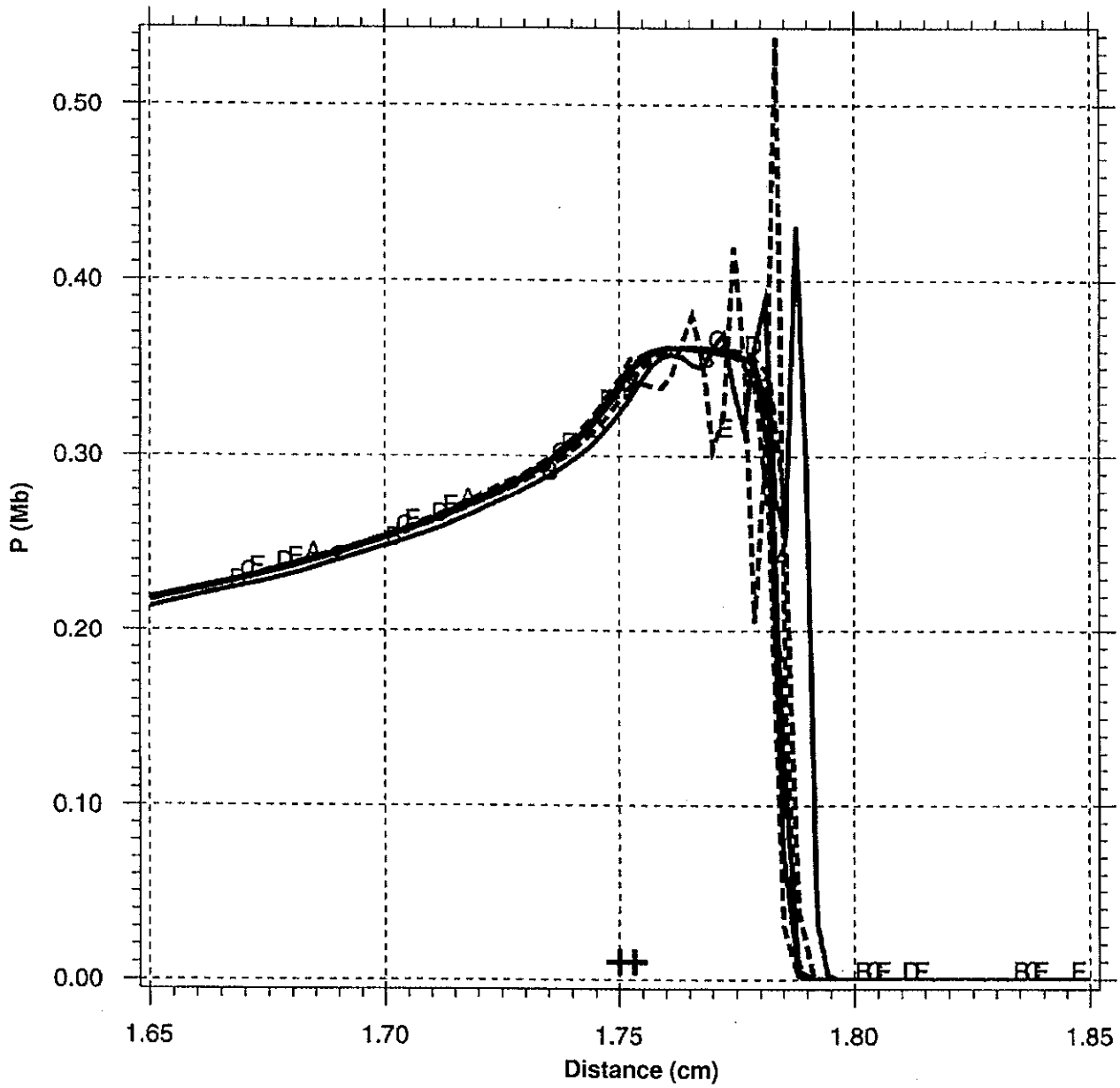

Figure D4. The effect of scalar Q (run m47, solid lines) and tensorial Q (run m49, dashed lines) for corner-centered velocities. The noisy profiles are on the 45° line where it is amplified by tensorial Q.

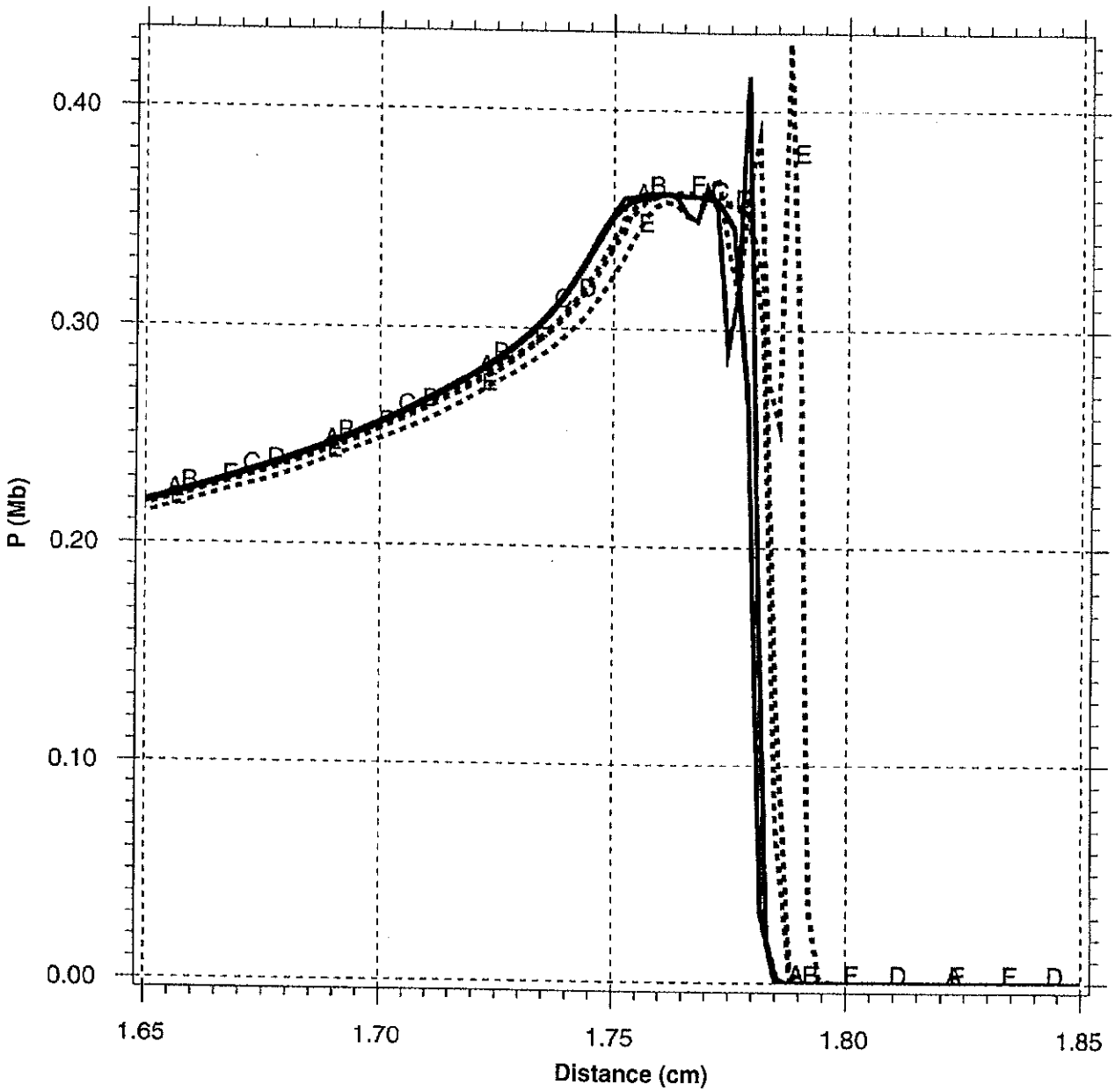

Figure D5. Pressure profiles for identical, Eulerian meshes when using corner-centered velocities with standard hydro (run m47, dashed lines) and with ALE hydro (run m64, solid lines). Both runs use scalar Q and the time is about 2.132 μs. Both runs generate a lot of noise on the 45° line but for the ALE run the three profiles are in closer agreement.

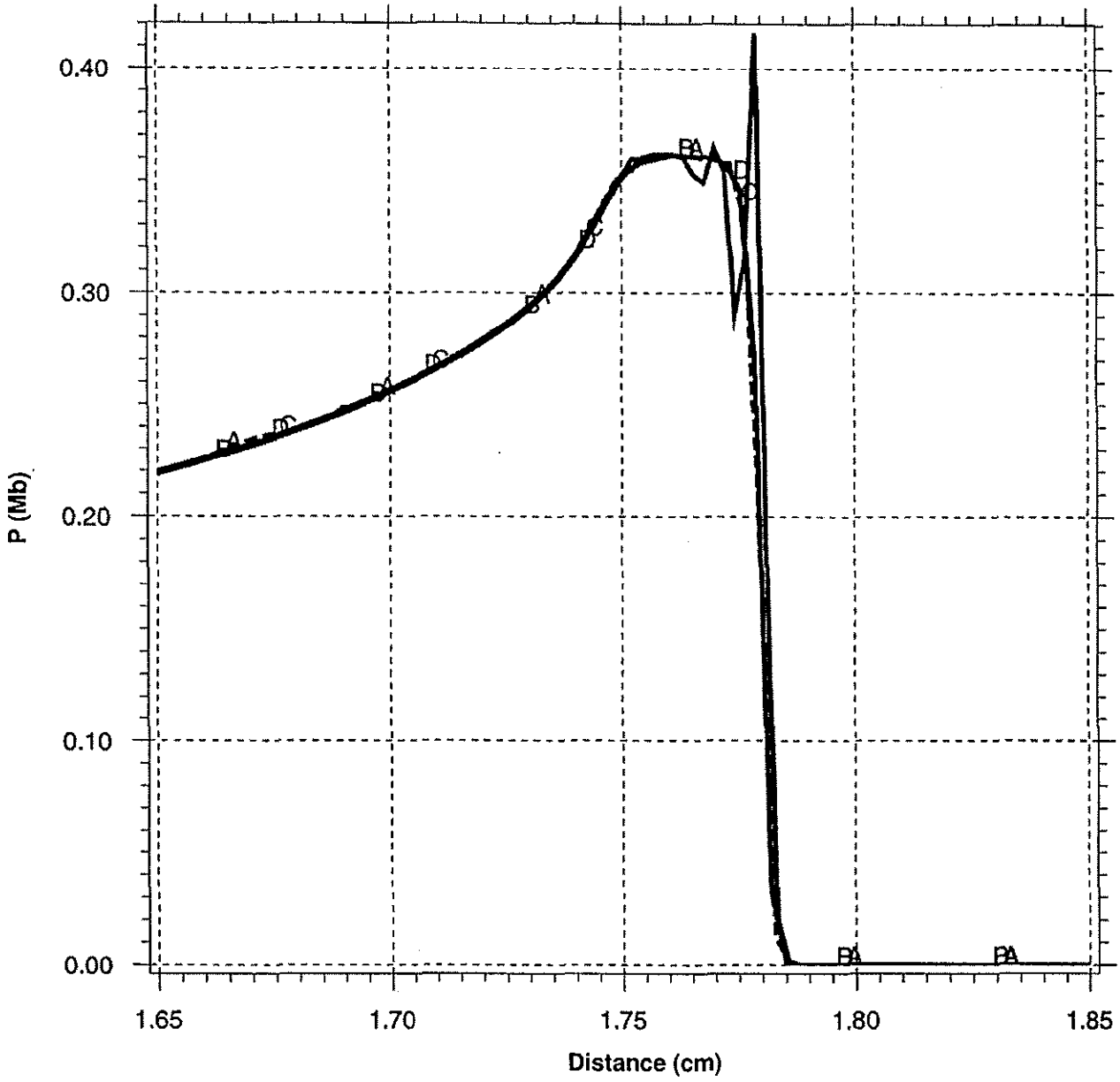

Figure D6. Pressure profiles for ALE hydro (run m64, solid lines) and run m65 (dashed line) comparing 2D ALE hydro results with 1D spherical metric results. Except for the overshoot on the 45° line in the ALE hydro, the results are judged to be the same.

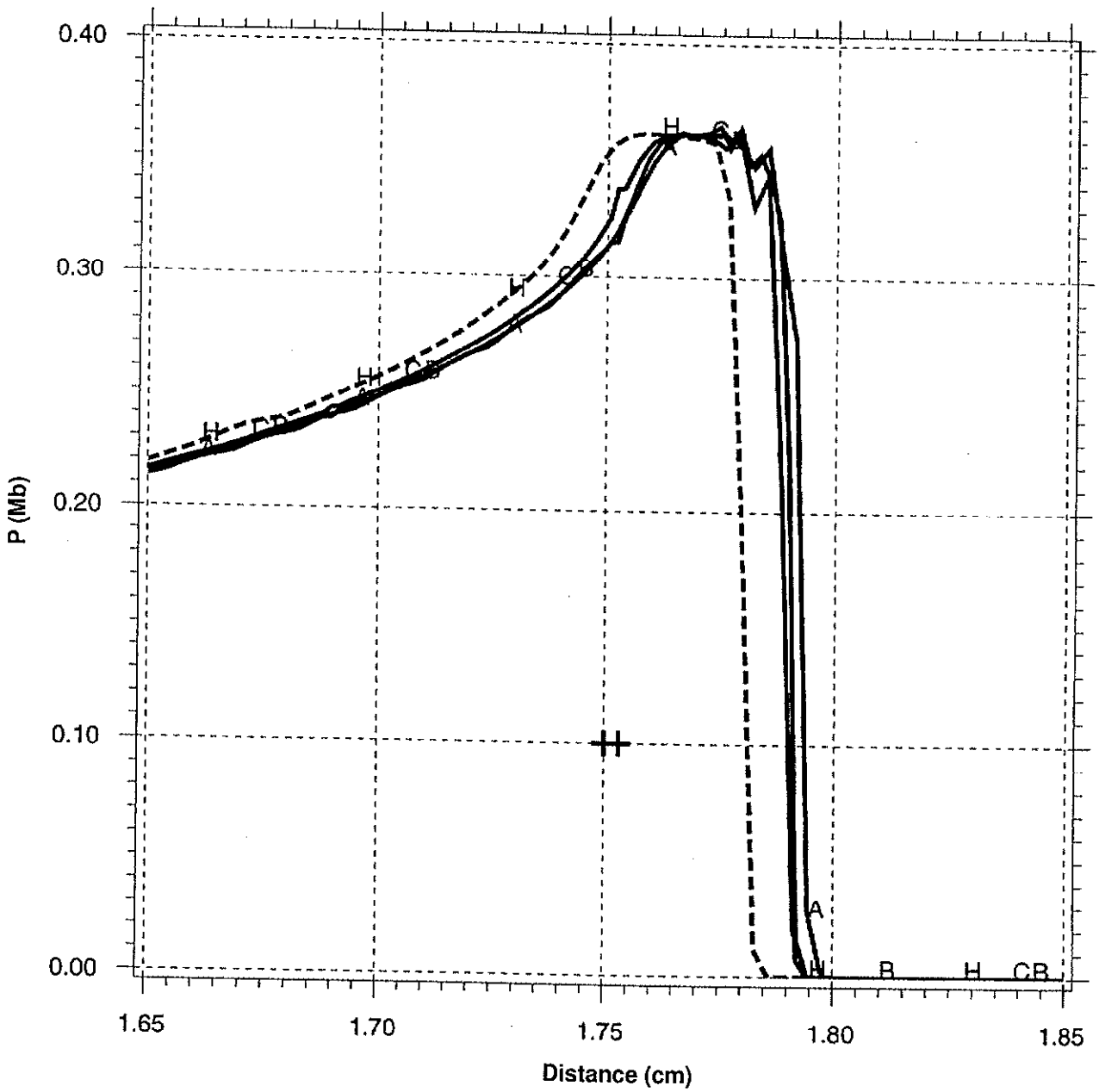

Figure D7. Pressure profiles comparing run 2D m43 at 3°, 45°, 97° (face-centered velocities, tensorial Q, solid lines) with run m65 (1D spherical metric, dashed line). The length of the relevent zone edge is indicated by the center-to-center distance between the two "plus" signs. Face-centered hydro with tensorial Q closely approximates results from 1D while minimizing internal inconsistencies and noise.

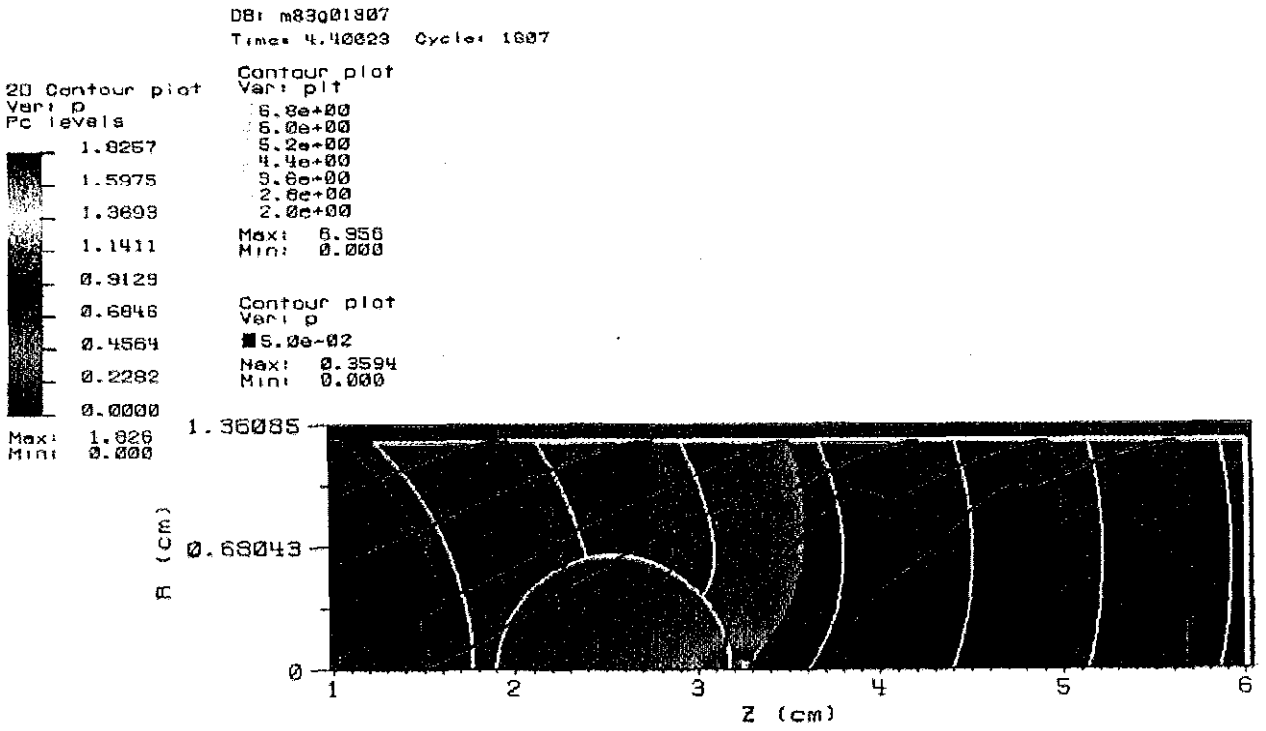

Figure E1. Contours of shock positions using reactive flow (run m83, red contours) and predicted shock positions using lighting times (yellow contours) every 0.8 μs beginning at 2.0 μs. Pseudo colors of pressures from reactive flow (run m83) are shown at t = 4.4 μs. The positions of the shock front in the reactive flow calculation is determined by the contour line corresponding to a pressure of 0.5 Mb. Portions of this contour that result from the open boundary are easily distinguished from the shock. The initial lag of the reactive flow front behind the lighting time front is apparently increased by the effects of shadowing.

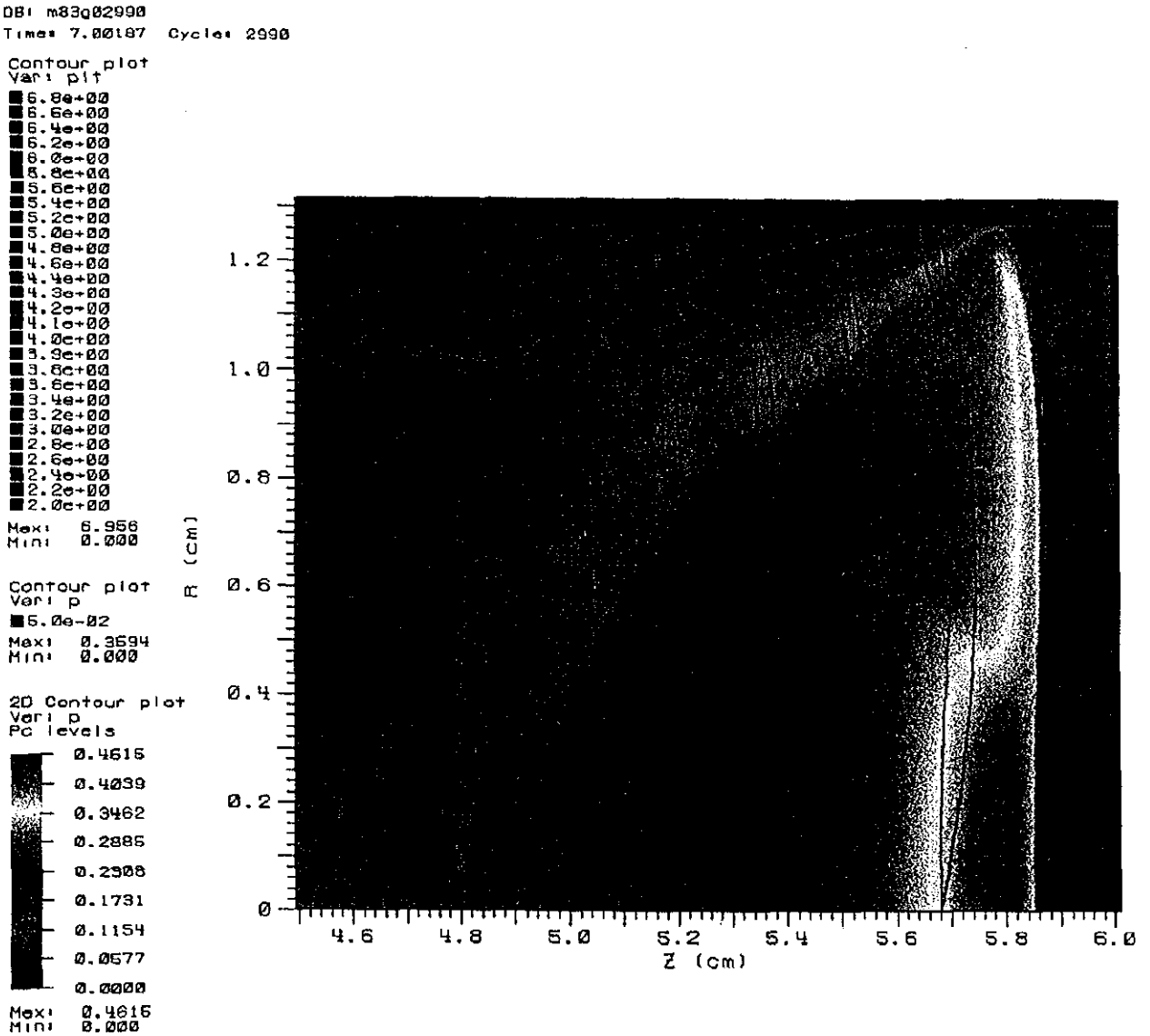

Figure E2. Comparison of predicted shock positions using lighting times (black contours, run m83) and positions of shock fronts calculated from reactive flow. A pseudo color plot of pressure calculated form reactive flow is shown at t = 7.0 μs. The contours are shown every 0.2 μs. The Mach stem is clearly visible and its growth can be inferred from the increasingly longer straight section in the reactive shock front near the axis of symmetry.

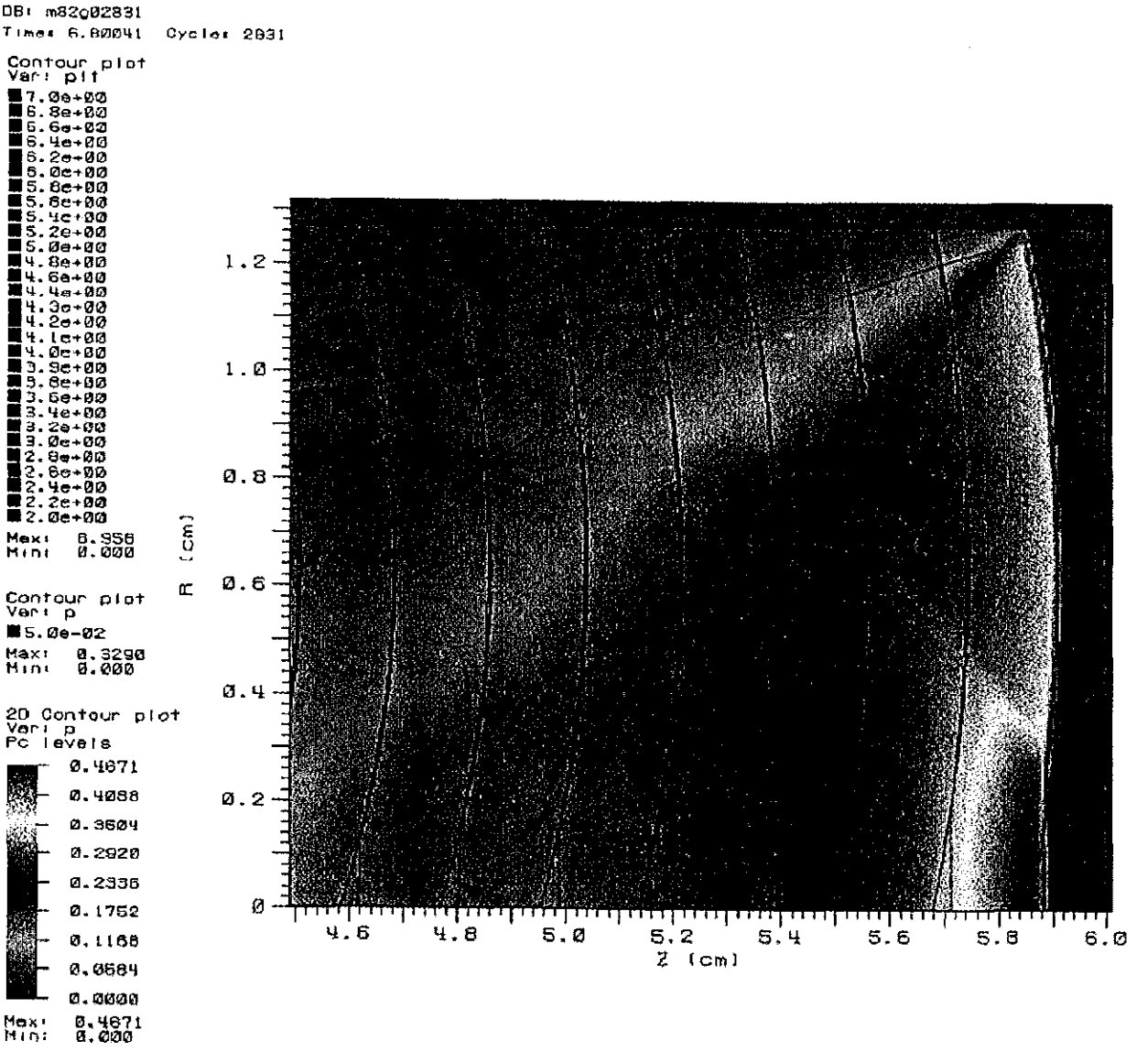

Figure E3. Positions of shock fronts predicted by lighting times (black contours) and positions of actual shock fronts obtained from a calculation (m82) that used lighting times assisted by beta burn. The pseudo color plot shows pressure values in the calculation (run m82) at t = 6.8 μs. Beta burn causes the Mach stem to advance more rapidly than programmed burn used alone.

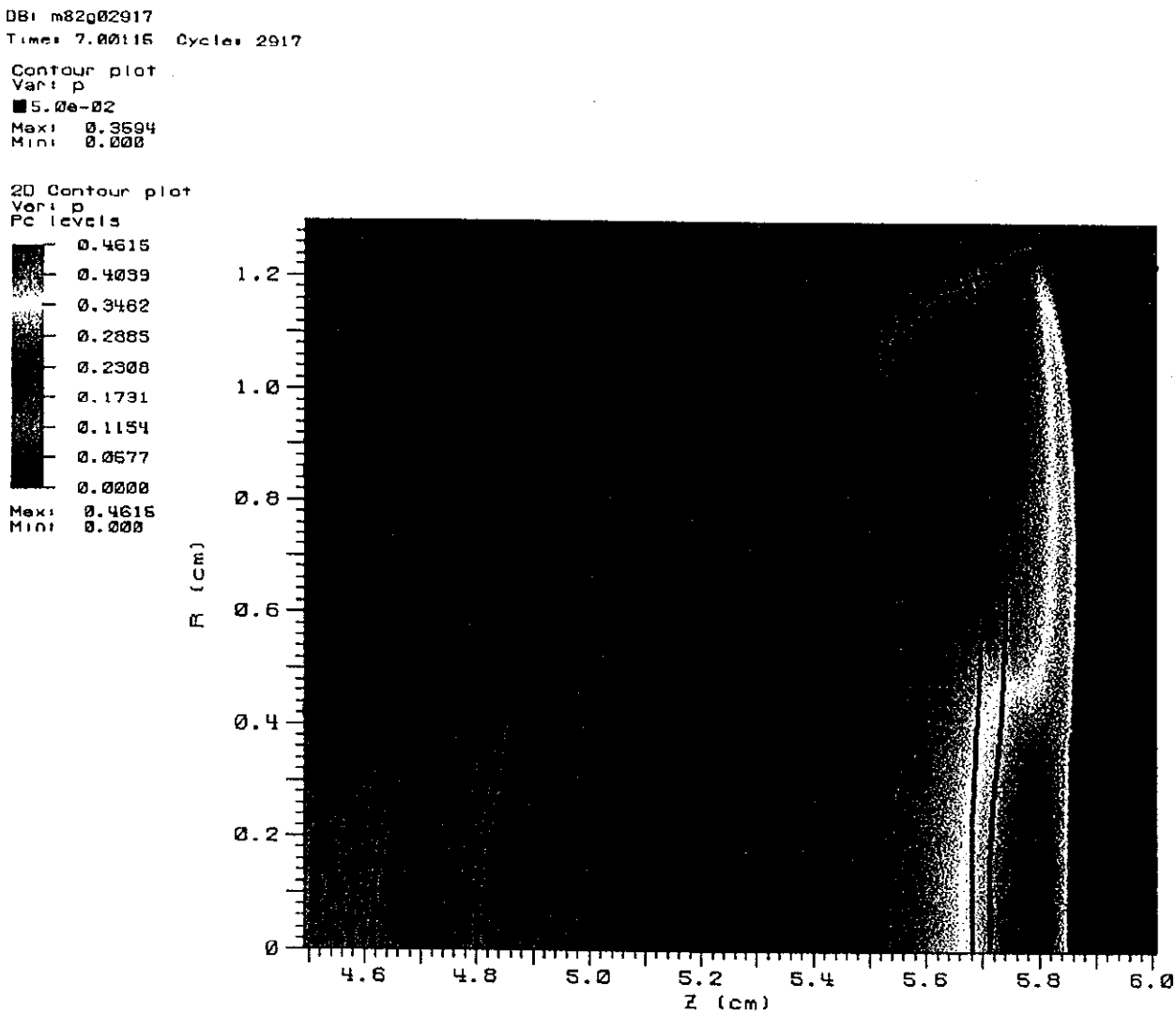

Figure E4. Positions of the shock front using beta-burn-assisted programmed burn (black contours, run m82) and using reactive flow (red contours, run m83). The pseudo color plot shows the pressures obtained from reactive flow at t = 7.0 μs. A comparison of the contours shows that reactive flow yields a more expansive Mach stem and a generally flatter shock front. An inspection of the contours near the axis (Mach stem region) suggests a slightly faster rate of travel for the Mach stem that is calculated by reactive flow than is indicated by the calculation using programmed burn.